이학박사학위논문

Prss14의 세포내 절편 생성과 그 기능에 대한 연구

Studies on the mechanism of regulated intramembrane proteolysis of Prss14 and Its role in cancer metastasis

2019년 2월

서울대학교 대학원
생명과학부
조영경

ABSTRACT

Studies on the mechanism of regulated intramembrane proteolysis of Prss14 and its role in cancer metastasis

Youngkyung Cho

School of Biological Sciences

The Graduate School

Seoul National University

Prss14 (Protease serine 14) is a type II transmembrane serine protease widely expressed in epithelial tissues. It has been reported that Prss14 is overexpressed in many cancers and plays critical roles in cancer initiation, progression, and metastasis. Prss14 undergoes ectodomain shedding in response to various stimulus including serum, TGF-β, and PMA. The fate of the membrane anchored N-terminal fragment (NTF) resulted from ectodomain shedding remains unknown. Here I show that the membrane-bound remnant, is subjected to regulated intramembrane proteolysis (RIP) and translocates to the nucleus. After PMA-induced ectodomain shedding of Prss14 mediated by tumor necrosis factor-α converting enzyme (TACE), the signal peptide peptidase-like 2b (SPPL2b) cleaves the N-terminal fragment. The generated soluble Prss14 intracellular domain (PICD) is liberated from the membrane and move

to the nucleus, where it regulates transcription. Strategic RNA-seq analyses revealed the PICD target genes including transcription factors, cytokines, migration and invasion-associated genes, and ubiquitin proteasome pathway-associated genes. The network analysis showed that these genes are well associated in three sub-networks centered on *Fos*, *Tnf*, and *Ubc*. PICD target genes are known for the functions of cell migration, invasion, epithelial-mesenchymal transition (EMT), and modulation of cancer microenvironment. The ability of cell invasion and migration is abolished when SPPL2b was knocked down and it is recovered by transfection of exogenous PICD (N55). Furthermore, the cells expressing Flag-tagged N55 show EMT-like scattered cellular morphology. In addition, the epithelial marker E-cadherin is decreased and mesenchymal marker Vimentin is increased in Flag-N55-expressed cells, demonstrating that PICD itself can induce EMT. The survival of estrogen receptor (ER)-negative breast cancer patients with high *PRSS14* expression is poorer in the patients with high level of *PRSS14* and *SPPL2B*. Also, ER-negative patients expressing high level of *PRSS14* and PICD target genes are able to use for the good prognosis markers for ER-negative breast cancer. Therefore, these results suggest that a novel mechanism of PICD to promote cancer metastasis by increasing cell invasion and EMT and modulating cancer microenvironment through transcriptional regulation. I propose that the dual function of Prss14 plays in cancer metastasis, by affecting target gene expression with intracellular

domain as well as by cleaving substrates with protease domain.

Keyword : Prss14, SPPL2b, Regulated Intramembrane Proteolysis, Transcriptional regulation, EMT, Metastasis

Student Number : 2011-20353

TABLE OF CONTENTS

LIST OF FIGURES

LIST OF TABLES

BACKGROUND

Prss14 in cancer progression

Proteases are involved in many processes of cancer progression. They degrade the extracellular matrix (ECM) molecules and allow the cancer cells to migrate basement membrane and invade into the surrounding tissues and vasculature. In many cancers, the proteases including cathepsins, matrix metalloproteases (MMPs), and serine proteases are upregulated (Affara et al., 2009; Deryugina and Quigley, 2006; Friedl and Wolf, 2003; Mohamed and Sloane, 2006; Netzel-Arnett et al., 2003). Recently, there have been many reports that proteases not only provide the way to migrate for cancer cells, but also activate pro-tumorigenic signaling pathway.

Among these proteases, the type II transmembrane serine protease (TTSPs) localized at the at cell surface have been known to play critical roles to cleave cytokines, growth factors, and receptors, such as VEGF, HGF, and uPAR and activate signaling pathways (Affara et al., 2009; Sevenich and Joyce, 2014). Cell surface localization allows TTSPs efficiently mediate signal transduction between the cancer cells and their surrounding environment.

Prss14 (Protease serine 14) is one of the most studied members of TTSPs. It is also known as epithin (Kim et al., 1999), matriptase (Lin et al., 1999b), ST14 (Zhang et al., 1998), and membrane type

serine protease 1 (MT-SP1) (Takeuchi et al., 1999). Prss14 has a multidomain structure, containing a short cytoplasmic tail, two Cls/Clr, urchin embryonic growth factor, bone morphogenetic protein (CUB) domains, four low-density lipoprotein receptor class A repeats, and serine protease domain (Fig. 1). The cytoplasmic domain has been reported to interact with filamin and translocate Prss14 to cell surface (Kim et al., 2005). The CUB domains and LDLRA repeats participate in zymogen activation (Inouye et al., 2013). In addition, second CUB domain interacts with HAI-1 and facilitates inhibitory interaction between Prss14 and HAI-1 (Inouye et al., 2010). LDLRA domains provide the specific binding sites for Tie2 and allow Prss14 to cleave Tie2 (Kim et al., 2011). Prss14 cleaves and activates diverse substrates, such as hepatocyte growth factor (HGF) (Lee et al., 2000), urokinase type plasminogen activator (uPA) (Lee et al., 2000), protease activated receptor (PAR) 2 (Takeuchi et al., 2000), epidermal growth factor receptor (EGFR) (Chen et al., 2008), Tie2 (Kim et al., 2011), MMP3 (Jin et al., 2006), prostasin (Netzel-Arnett et al., 2006), and extracellular matrix proteins (Tripathi et al., 2011). Its proteolytic activity is regulated by a Kunitz-type serine protease inhibitors, hepatocyte growth factor activator inhibitor 1 and 2 (HAI-1 and HAI-2) (Lin et al., 2008; Szabo et al., 2008). HAIs are co-expressed with Prss14 in epithelium and tightly regulate proteolytic activity of Prss14 (Oberst et al., 2001)

Figure 1. Domain structure of Prss14

Prss14 has a multidomain structure, containing a short cytoplasmic tail, two Cls/Clr, urchin embryonic growth factor, bone morphogenetic protein (CUB) domains, four low-density lipoprotein receptor class A repeats, and serine protease domain

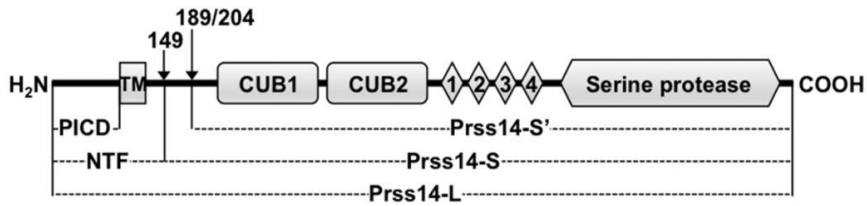
189/204
149
H2N
TM
CUB1
CUB2
1
2
3
4
Serine protease
COOH
PICD
Prss14-S'
NTF
Prss14-S
Prss14-L

Prss14 is expressed almost epithelial tissues. Its upregulation has been shown in variety of human epithelial cancers, such as breast, prostate, ovary, cervix, colon, and esophagus, indicating the critical roles in cancer initiation and progression (List, 2009; Uhland, 2006). Furthermore, increased Prss14 expression was tightly linked to tumor grade and poor survival in cancer patients (Chang et al., 2013; Ha et al., 2014; Kang et al., 2003; Kim et al., 2016; Lee et al., 2005; Oberst et al., 2001; Oberst et al., 2002; Saleem et al., 2006; Tsai et al., 2014). Transgenic mice expressing Prss14 in the epidermis by K5-promoter showed spontaneous cell carcinogenesis, suggesting the direct evidences that Prss14 was involved in cancer initiation and development (List et al., 2005). Another animal studies showed that mice injected with cells increased Prss14 presented remarkable increased angiogenesis, invasive growth, and metastasis (Ihara et al., 2002; Jin et al., 2006). Conversely, tumor formation and metastasis were severely impaired in injected by cells with reduced Prss14 expression or activity (Cheng et al., 2013; Kim et al., 2011; Ko et al., 2015; List et al., 2005; Steinmetzer et al., 2006; Tsai et al., 2014).

In our previous studies, the soluble secreted form of Prss14 could induce angiogenesis by increasing the migration, invasion of endothelial cells (Kim et al., 2010). Prss14 cleaved and activated Tie2 on endothelial cells to enhance the TEM of cancer cells (Kim et al., 2011). Prss14-dependent TEM was also observed in activated macrophages (Lee et al., 2011). In addition to these extracellular functions, Prss14 expression itself induced mesenchymal

characteristics in MDCK epithelial cell line accompanied by genetic reprograming within these cells (Lee et al., 2010). However, how intracellular changes are induced by Prss14 overexpression remains unclear.

Prss14 undergoes multiple processing steps

Prss14 undergoes series of proteolytic processing steps prior to becoming a functional protease by autocatalysis at Arg614 (Uhland, 2006). Prss14 synthesized as a single-chain zymogen is cleaved at Gly149 to produce two fragments, N-terminal fragment (NTF) and Prss14-S, which are non-covalently associated on the membrane (Cho et al., 2001). The protein is shed from the membrane by cleavage at Arg186, Lys189, or Lys204. This shedding is induced by various stimuli such as the serum (Benaud et al., 2001), phorbol 12-myristate 13-acetate (PMA) (Kim et al., 2005), transforming growth factor-β (TGF-β) (Lee et al., 2014), hypoxia (Kim et al., 2010), and acidic conditions (Tseng et al., 2017). The ectodomain shedding is mediated by TACE/ADAM17 (Cho et al., 2017; Lee et al., 2014) and/or serine protease, possibly Pss14 itself (Tseng et al., 2017). However, the fate of the remaining N-terminal fragment (NTF) of Prss14 resulting from ectodomain shedding is unknown.

Figure 2. Multiple processing steps of Prss14

Prss14 is synthesized as a single-chain zymogen and cleaved at Gly149 to produce two fragments, N-terminal fragment (NTF) and Prss14-S, which are non-covalently associated on the membrane in ER. After this N-terminal processing, Prss14 is shed from the membrane by cleavage at Arg186, Lys189, or Lys204 upon various stimuli such as serum, PMA, TGF-β, hypoxia, and acidic buffer.

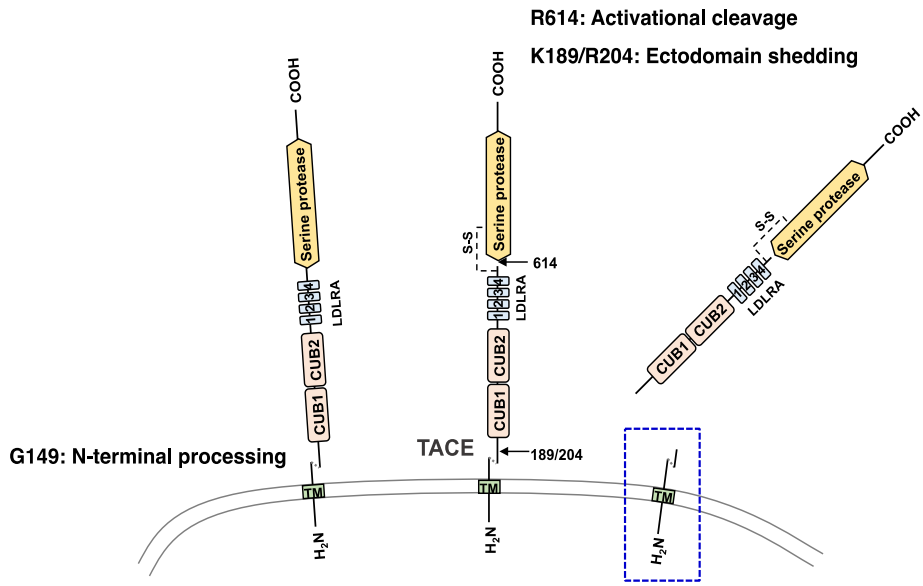
R614: Activational cleavage
K189/R204: Ectodomain shedding
COOH
Serine protease
S-S
614
LDLRA
CUB2
CUB1
TACE
189/204
G149: N-terminal processing
TM
H2N

Regulated intramembrane proteolysis

Some membrane proteins undergoing ectodomain shedding is further processed by regulated intramembrane proteolysis (RIP). RIP has received considerable attention as the fundamental process producing messengers for signal transduction and affecting the diverse cellular processes, such as cell differentiation, proliferation, apoptosis, and neurogenesis (Brown et al., 2000; Lal and Caplan, 2011). RIP is generally preceded by initial ectodomain shedding and cleaves the membrane-bound remnant. After this cleavage, the generated intracellular domain (ICD) is liberated from membrane (Fig.3). This released ICD functions as a signaling molecule in cytosol or a transcriptional regulator after translocation to the nucleus (Brown et al., 2000).

The intramembrane protease to carry out RIP includes three distinct protease families, the site-2 protease-type metalloproteases, the rhomboid serine proteases, and Presenilins and signal peptide peptidase (SPP)-type aspartic proteases (Weihofen and Martoglio, 2003). In the aspartic protease family, presenilins and SPP-like proteases (SPPLs) strictly prefer to cleave the type I and type II transmembrane protein, respectively (Fluhrer et al., 2009). Each SPPL members is localized in different subcellular compartments: SPPL2a in the lysosome and late endosomes, SPPL2b in the plasma membrane, SPPL2c in the ER, and SPPL3 in the Golgi. In line with their distinct localization, it is thought that each member is involved in the specific cellular process with unique substrates

Figure 3. Regulated intramembrane proteolysis

After ectodomain shedding, some transmembrane proteins are subjected to intramembrane cleavage to generate intracellular domain (ICD). This ICD liberated from membrane is degraded or functions as a signaling molecule in cytosol, or translocate to the nucleus, where it participates gene transcription.

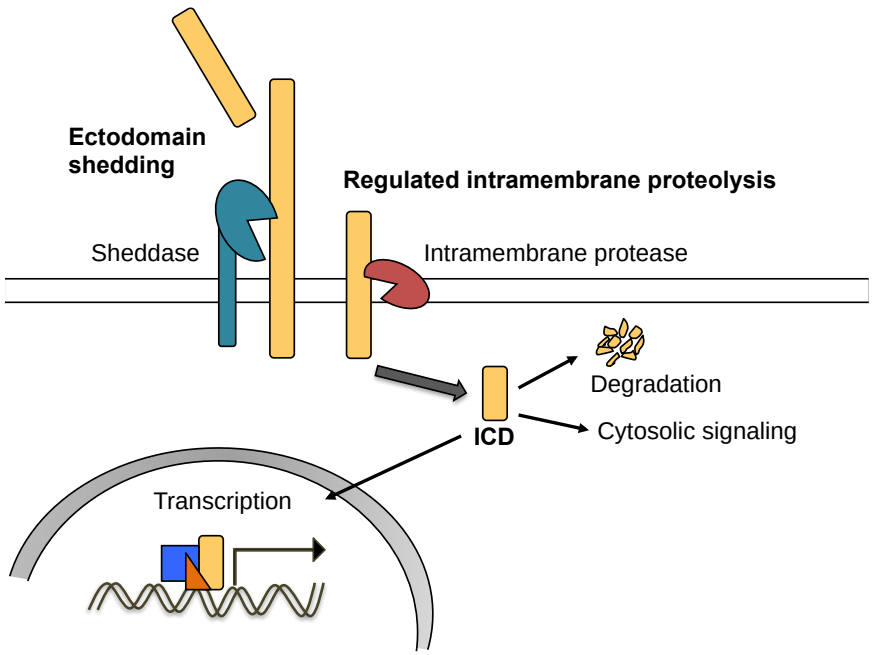
Ectodomain
shedding
Regulated intramembrane proteolysis
Sheddase
Intramembrane protease
Degradation
ICD
Cytosolic signaling
Transcription

(Friedmann et al., 2006; Krawitz et al., 2005; Voss et al., 2013)

The improper control of RIP leads to various diseases (Lal and Caplan, 2011; Lichtenthaler et al., 2011). Too much RIP of amyloid precursor protein (APP) by presenilin can lead to the Alzheimer's disease (Hardy and Selkoe, 2002). For epithelial cell adhesion molecule (EpCAM), dysregulated RIP promotes the cancer initiation and progression upregulating genes involved in cell proliferation, stemness, and EMT (Hsu et al., 2016; Lin et al., 2012; Maetzel et al., 2009).

INTRODUCTION

Metastasis is a multistep process including angiogenesis, epithelial mesenchymal transition (EMT), migration, invasion, transendothelial migration (TEM), and colonization in secondary organs (Chambers et al., 2002; Gupta and Massague, 2006). Especially, EMT involves the massive changes in gene expression profiles and is the critical process to confer highly increased motility and invasiveness. EMT is driven by the EMT-inducing transcription factors, such as well studied *SNAI1*, *SNAI2*, *TWIST1*, *ZEB1*, and *ZEB2* (Thiery, 2002; Yang and Weinberg, 2008). More transcription factors including *SOX4* and *RUNX* besides these transcription factors were also demonstrated to induce the EMT process (Lourenco and Coffer, 2017; Voon and Thiery, 2017). In addition, editing of cancer by immune cells is important during cancer progression and metastasis. Cancer cells modulate the immune system to create favorable tumor microenvironment for cancer. Cytokines produced by the cancer cells are the key mediators to escape the immune response and to further facilitate the metastatic steps (Kitamura et al., 2015; Schreiber et al., 2011).

Prss14 (Protease serine 14), also known as epithin (Kim et al., 1999), matriptase (Lin et al., 1999b), ST14 (Zhang et al., 1998), and membrane type serine protease 1 (MT-SP1) (Takeuchi et al., 1999), is a type II transmembrane serine protease that plays multiple critical

roles during cancer metastasis processes. Many studies showed that Prss14 was upregulated in variety of human epithelial cancers, such as breast, prostate, ovary, cervix, colon, and esophagus (List, 2009; Uhland, 2006). Its increased expression was tightly linked to higher tumor grade and poor survival in patients (Chang et al., 2013; Friis et al., 2014; Kang et al., 2003; Kim et al., 2016; Lee et al., 2005; Oberst et al., 2001; Oberst et al., 2002; Saleem et al., 2006; Tsai et al., 2014). In previous studies, it was demonstrated that Prss14 had crucial functions in every steps of metastasis. The soluble secreted form of Prss14 could promote angiogenesis by enhancing migration, invasion, and tube formation of endothelial cells (Kim et al., 2010). In addition, overexpression of Prss14 induced EMT, thereby increased cell migration and invasion and TGF-β-induced EMT was observed in Prss14-dependent manner (Lee et al., 2010). These results imply its essential role in EMT but the mechanism underlying Prss14-mideated EMT remains still unknown. Prss14 also enhanced TEM of cancer cells by cleaving and activating Tie2 (Kim et al., 2011). Furthermore, metastasis was severely impaired in mice injected by breast cancer cells with reduced Prss14 level (Kim et al., 2011). In another studies, downregulation of Prss14 and inhibition of its activity significantly reduced metastasis in xenograft mice model (Cheng et al., 2013; Ko et al., 2015; Steinmetzer et al., 2006; Tsai et al., 2014). Conversely, when cancer cells with increased Prss14 or active form of Prss14 were grafted to immunodeficient mice, remarkable increased angiogenesis, invasive growth, and metastasis

were observed (Ihara et al., 2002; Jin et al., 2006). The transgenic mice expressing Prss14 in the epidermis showed the increased invasive tumor growth and metastasis in presence of carcinogen (List et al., 2005). This mice model also displayed spontaneous squamous cell carcinogenesis, indicating that Prss14 was also required for tumor initiation and tumor growth. Another mice model that genetically reduced Prss14 expression showed severely impaired tumor formation and growth (Zoratti et al., 2015).

Prss14 undergoes series of proteolytic processing to be a functional protease (List et al., 2006). During biogenesis, Prss14 synthesized as a single chain zymogen is cleaved at Gly149 and becomes the membrane-localized form in which cleaved extracellular region is non-covalently associated with N-terminal fragment (NTF) (Cho et al., 2001). To possess proteolytic activity, Prss14 is further cleaved at Arg614 in autocatalytic fashion and converted to two-chain active protease (List et al., 2006). The active Prss14 is tightly regulated by its cognate inhibitors, hepatocyte growth factor activator inhibitor 1 and 2 (HAI-1 and HAI-2) (Lin et al., 1999; Szabo et al., 2008). In addition, a cleavage at Lys189 or Lys204 occurs and releases the ectodomain containing 2 CUB domains, 4 LDLRA repeats, and protease domain from cell surface (List et al., 2006). After this shedding, Prss14 N-terminus including short stem region, transmembrane domain, and intracellular domain remains in the membrane. Ectodomain shedding is induced by various stimuli such as serum (Benaud et al., 2001), PMA (Kim et al.,

2005), TGF-β (Lee et al., 2014), hypoxia (Kim et al., 2010), and acidic buffer (Tseng et al., 2017). The ectodomain is cleaved by tumor necrosis factor-alpha-converting enzyme (TACE/ADAM17) upon PMA and TGF-β, showing that knockdown of TACE significantly inhibited the ectodomain shedding (Cho et al., 2017; Lee et al., 2014). As well as TACE activity, serine protease activity is closely linked to shedding process because the Prss14 catalytic inactive mutants does not undergo ectodomain shedding in acidic buffer (Tseng et al., 2017) and serine protease inhibitors also reduce the Prss14 shedding (Cho et al., 2005; Kim et al., 2005). In PMA-induced shedding, Prss14 activation and ectodomain shedding are induced after rearrangement of actin cytoskeleton and translocation of Prss14 to the cell-cell contact through direct interaction between its intracellular domain and filamin, indicating the roles of intracellular domain in translocation, activation, and shedding (Kim et al., 2005). Besides these roles, function of intracellular domain has not been studied.

Some membrane proteins undergoing ectodomain shedding is processed by regulated intramembrane proteolysis (RIP) (Brown et al., 2000; Lal and Caplan, 2011). RIP is typically followed by initial ectodomain shedding and generates the soluble intracellular domain (ICD). This generated ICD functions as a signaling molecule in cytosol or a transcriptional regulator after translocation to the nucleus. (Brown et al., 2000).

In this study, I report the biological function of Prss14

intracellular domain in cancer metastasis. I show that SPPL2b cleaves N-terminal fragment of Prss14 followed by PMA-induced ectodomain shedding and generates PICD, which promotes migration, invasion, and EMT through transcriptional regulation.

MATERIALS AND METHODS

Cell lines

427.1.86 (Cho et al., 2001), MCF7, and HEK293T cells were maintained in DMEM (Gibco) with 10% FBS (Gibco) and 1% penicillin/streptomycin (P/S) (Gibco). CHO-K1 cells were maintained in F-12 nutrient mixture medium (Gibco) with 10% FBS and 1% P/S. 4T1 cells were maintained in DMEM (Welgene) with 10% FBS and 4mM L-glutamine (Welgene), and 1% P/S. To generate the SPPL2b knockdown 427.1.86 cell lines, two constructs containing SPPL2b RNAi and selected more effective construct (pSUPER-SPPL2b-2). The pSUPER-SPPL2b-2 was transfected into 427.1.86 cells with pcDNA3 vector. After growing in the presence of 800 μg/ml G418 (Welgene), clones derived from single cells in 96 well were tested for their SPPL2b expression in RNA level with qPCR. For Flag-N55 cell lines, p3XFlag-Prss14 N55 was transfected into 427.1.86 cells and selected with 800 g/ml G418. Clones derived from single cells in 96 well were tested for their Flag-N55 expression in protein level by western blot analysis with anti-Flag antibody. For control cell lines, pSUPER vector (CONT) and p3XFlag vector (VEC) were transfected into 427.1.86 cells. Lipofectamine PLUS Transfection Reagent (Thermo Fisher Scientific, 11514-015) was used for all transfection experiments. Cells were cultured at 37℃ in a 5% CO2.

Plasmid and siRNA

The PCR fragments were cloned into the NotI/BamHI sites of the p3XFlag-CMV10 vector (Sigma): full length Prss14, amino acids 1–55, 1–149, 1–162, and 1–213. All Prss14 constructs were designed to be in-frame with an N-terminal Flag tag (Fwd: 5'-AGAGCGGCCGCAATGGGTAGCAAT-3', N55 Rev: 5'-ACAGGATCCCCAAGCGCCTGGGGC-3', N149 Rev: 5'-ACAGGATCCCTCACTGAAGGCAGTT-3', N162 Rev: 5'-ACAGGATCCGGGGATGCTGAACTC-3', N213 Rev: 5'-TGTGGATCCGCTGTTGTCCTGAGT-3', and Wild type Rev: 5'-ACAGGATCCCTATACCCCAGTGTG-3'). Human SPPL2b cDNA was purchased from OriGene. SPPL2b C-terminally tagged with HA sequence was cloned into the KpnI/EcoRI sites of the pcDNA3 vector SPPL2b-HA-Fwd: 5'-GGGGTACCAAAATGGCGGCAGCGGTG-3' and Rev: 5'-GGAATTCCTTAAGCATAATCTGGAACATCATATGGATAGGCCG AGGCGCCAGG-3'. Flag-Prss14G73A construct was generated by PCR mutagenesis using p3XFlag-Prss14 and QuikChange II XL Site-Directed Mutagenesis Kit (Agilent) for amino acid substitutions according to the manufacturer's instructions. To generate pSUPER-SPPL2b-2, a pair of oligonucleotides containing a target sequence in mouse SPPL2b (Fwd: 5'-GATCCCCCCGAGCAGCCTCCAAGTGATTCAAGAGATCACTTGGA

GGCTGCTCGGTTTTTA-3' and Rev: 5'-TCGATAAAAACCGAGCAGCCTCCAAGTGATCTCTTGAATCACT TGGAGGCTGCTCGGGGG-3') was cloned into pSUPER (OligoEngine).

Immunocytochemistry

Cells grown on gelatin coated slide cover were fixed with 3.7% paraformaldehyde in PBS for 10 min, permeabilized with 0.1% TritonX-100 in PBS (PBS-T) for 30 min, and incubated in blocking solution (10% goat serum, 1% gelatin, and 0.1% TritonX-100 in PBS) for 30 min. After washing with PBS-T, samples were treated with primary antibody in blocking solution for 1 h. The following primary antibodies were used: rabbit polyclonal anti-Prss14 C-terminus, rabbit polyclonal anti-Prss14 N-terminus (Cho et al., 2001), mouse monoclonal anti-Flag (clone M2, Sigma, CP2983), rabbit polyclonal anti-HA (Santa Cruz Biotechnology, sc-805), mouse monoclonal anti-E-cadherin (clone 36, BD Biosciences, 612131), and mouse monoclonal anti-Vimentin (clone V9, Sigma-Aldrich, V6389). Cells then were washed with PBS-T and incubated with FITC- or TRITC-conjugated secondary antibodies (Jackson ImmunoResearch, 711-095-152, 715-095-150, 711-025-152, and 715-025-150) for 50 min. For actin staining, rhodamine-phalloidin (Molecular Probe, R415) was used. For EMT marker detection, cells were fixed on 2 days after seeding in growth medium. Finally, the coverslips

were mounted with DAPI (VECTASHIELD, H-1500) and observed under the fluorescence microscope (Axioplan200 M, Carl Zeiss). Images were processed in Photoshop CS6 (Adobe).

Western blot and immunoprecipitation analysis

Cells were incubated with 20 μM TAPI-0 (Calbiochem, 579050) for 2 h or 10 μM $(Z-LL)_2$ketone (Calbiochem, 421050) for 6 h in serum free medium. Then cells were incubated with 1 μM PMA (Sigma, P1585) for another 2 h. For control, diluent DMSO was treated. Cells were lysed with lysis buffer (50 mM HEPES (pH7.4), 150 mM NaCl, 1% NP-40, 0.5% Sodium deoxycholate, 1 mM EDTA in the presence of protease inhibitors, leupeptin, aprotinin, and pepstatin. Immunoprecipitation of Prss14 N-terminus was performed by antibodies and protein A Sepharose bead mixtures for 2 h, at 4℃. The immunoprecipitates were resuspended in LDS sample buffer and reducing agent (Invitrogen). Transfected cells were lysed with the lysis buffer and prepared in LDS sample buffer and reducing agent. After incubating for 10 min at 70℃, samples were resolved in a 4-12% NuPAGE gradient gel (Invitrogen, NP0335PK2). 10% trichloroacetic acid (TCA)-precipitates from medium were dissolved in SDS sample buffer under recuing condition and resolved in 9% SDS-PAGE gel. Samples were subjected to western blot analysis with using Enhanced Chemiluminescence reagents (Supersignal West Femto, Thermo, 34095). The following primary antibodies were used:

rabbit polyclonal anti-matriptase (Millipore, IM1014), mouse monoclonal anti-β-tubulin (clone TUB2.1, Sigma, T4026), Rabbit polyclonal anti-Laminin A/C (Cell Signaling, 2032), mouse monoclonal mAb5 (Cho et al., 2001), rabbit polyclonal anti-Prss14 N-terminus, rabbit polyclonal anti-human Prss14 N-terminus, mouse monoclonal anti-Flag, rabbit polyclonal anti-HA, mouse monoclonal anti-E-cadherin, and mouse monoclonal anti-Vimentin..

RNA extraction and quantitative PCR

Total RNA was extracted using TRIzol (Thermo Fisher Scientific) according to the manufacturer's recommendations. Reverse transcription reactions were performed with Superscript III Reverse Transcriptase (Thermo Fisher Scientific, 18080093). The primers sequences used for this study are listed in Resources Table. PCR amplifications were performed with TaqMan Gene Expression Master Mix (Thermo Fisher Scientific, 4369016) on StepOnePlus Real-Time PCR System (Applied Biosystems).

RNA-sequencing and data analysis

427.1.86-SPPL2b-knockdown control cells (CONT) and SPPL2b-knockdown cells (SP2bKD-10) were incubated in serum free medium, followed by another 2 h with or without 1 μM PMA.

After treatment with PMA, cells were washed with PBS and total RNA was extracted using TRIzol. p3XFlag vector or p3xFlag-N55 was co-transfected with GFP vector into SP2bKD-10 cells. After 24 h of transfection, GFP-positive cells were sorted using FACSAria II (BD Bioscience) (EGFP positive cells of 93% and 88% for KD/GFP and KD/GFP+N55, respectively). The collected GFP-positive cells were immediately lysed with TRIzol and RNAs were extracted. Quality control of extracted RNA was performed using Agilent 2100 BioAnalyzer with RNA Integrity Number (RIN) value greater than 9. RNA-seq was performed by TheragenEtex Bio Institute (Suwon, Korea) using with Illumina HiSeq 2500 paired-end RNA sequencing. Reads were aligned with Tophat (v2.1.1) and Fragments per kilobase of exon per million reads (FPKMs) were calculated using Cufflinks (v2.1.1). Cuffdiff (v2.1.1) was used for normalization. Before logarithmic processing, 0.000001 was added to FPKM values to all 6 samples and analyzed in density plots, 0.001 was chosen for FPKM cutoff to remove genes with no expression. To screen PICD target genes, we filtered out uncharacterized genes without known function and DEG analysis was performed pairwise. DEGs in both conditions were selected with p-value threshold of 0.1. Among these genes, genes with only the same directional changes in both DEG analysis were considered for further selection. DEG analysis was performed using edgeR (Robinson et al., 2010) . Final PICD target gene list satisfying all the criteria was analyzed to investigate their biological function.

Network and cellular process analysis

For network analysis of PICD target genes, STRING (Szklarczyk et al., 2015) was used. STRING predicted protein-protein interactions including physical interactions, as well as functional interactions from automated text-mining and computational predictions. Pathway Studio (Nikitin et al., 2003) based on in-depth literature mining analyzed the association between target genes and cell migration and invasion process ($p<0.001$). Promoter binding sites within PICD target genes of transcription factors were searched using ENCODE (Consortium, 2012).

Wound healing assay and invasion assays

For wound healing assays, cell monolayers were maintained in serum-free medium for 12 h and scratched using a P200 pipet tip. Cells were washed to remove cell debris and incubated in 1% serum-containing medium for 24 h. Photographs were taken at 0 and 24 h after wounding using Axiovert 200M and the area covered by migrating cells was determined by the ratio of scratch area at 0 h to scratch area at 24 h using ImageJ Software. Invasion assay was performed using a BioCoat Matrigel Invasion Chamber (Corning, 354480) according to the manufacturer's instructions. Cells were

maintained in serum-free medium for 12 h and 3×105 cells were seeded in serum-free medium into the upper chamber. The lower chamber was filled with DMEM containing 2% serum with or without 1 μM PMA. After 24 h of incubation, the cells on the upper surface of the membrane were removed using cotton swabs. The invaded cells on the lower surface of the membrane were fixed with 100% methanol for 10 min and stained with 0.2% crystal violet for 5 min. The invaded cells were counted under Axioimager M1 and fifteen fields were counted. The total number of cells was divided by the number of counted field in each assay.

Cell scattering assay

Flag vector and Flag-N55-expressing cells were seeded at a low density on 60mm dishes in triplicate and were allowed to grow in growth medium for 2 days. Brightfield images were taken at 200x magnification using fluorescence microscope (Axioplan200 M, Carl Zeiss). Cells were counted as the scattered when cells lost contact with neighboring cells and exhibited a migrating phenotype. More than 50 images were randomly selected. At least 700 cells were counted per each condition.

Data analyses using TCGA

TCGA data were downloaded using the Broad Institute's Firehose, web portal site that has been developed aiming to deliver automated analyses of the TCGA data to general users. We used Level 3 normalized RNA-seq data from the January 28, 2016 standard data run (https://doi.org/10.7908/C11G0KM9) (Center, 2016). Association between PICD target gene set and PRSS14 expression in breast cancer patients was analyzed using Gene Set Enrichment Analysis (GSEA v3.0, available online: http://www.broad.mit.edu/gsea/) (Subramanian et al., 2005). For expression correlation analysis, expression values of all patients were drawn in scatter plots with linear interpolation curves between the two genes. The correlation coefficient r values between two genes were calculated using Pearson correlation and unpaired two-tailed students t-test was performed. For the 5 years survival rate, Kaplan-Meier survival analysis was used using TCGA breast cancer data excluded data whose contacts were lost in 5 years. The p values were calculated using a Log-rank (Mantel-Cox) test and the hazard ratio (HR) was determined by the Mantel-Haenszel method.

RESULTS

N-terminal of Prss14 is localized in the nucleus

Prss14 underwent multiple posttranslational processing and I wanted to know the cellular localization of two ends of the protein after this processing. The N-terminal and C-terminal region were detected in the normal culture condition using 427.1.86 thymoma cell expressing Prss14 endogenously. When the antibody binding to the extracellular part (C-terminus) showed the membrane staining, located in the cell-cell contacts, the antibody binding to the intracellular part (N-terminus), interestingly, showed nuclear staining (Fig. 4A). Both membrane staining and nuclear staining were disappeared Prss14-knockdown 427.1.86 cells, validating the specificity of these antibodies (Fig. 4B). The expression of Prss14 in knockdown cells was shown in Fig. 4C. Nuclear localization of the Prss14 N-terminus was further verified with ectopically expressing the Flag-tagged intracellular domain (N-terminal 55 amino acids) in COS7 cells (Fig. 5). These findings suggest that the Prss14 N-terminus maybe detach from the plasma membrane and translocate to the nucleus.

Ectodomain shedding induces PICD generation

As some membrane proteins undergoing ectodomain shedding

Figure 4. C-terminus and N-terminus of Prss14 show different cellular localization in 427.1.86 cells

(A) Cellular localization of endogenous Prss14 in 427.1.86 cells. Anti-Prss14 antibodies (green) against extracellular parts (anti-C antibody) or intracellular parts (anti-N antibody) were used. Scale bars, 20 μm. (B) Prss14 was stained with two kinds of anti-Prss14 antibodies in 427.1.86 cells (427) and 427.1.86-Prss14 knockdown cells (427KD). Scale bars, 20 μm. (C) Western blot analysis of Prss14 in 427KD cells using mAb5 antibody.

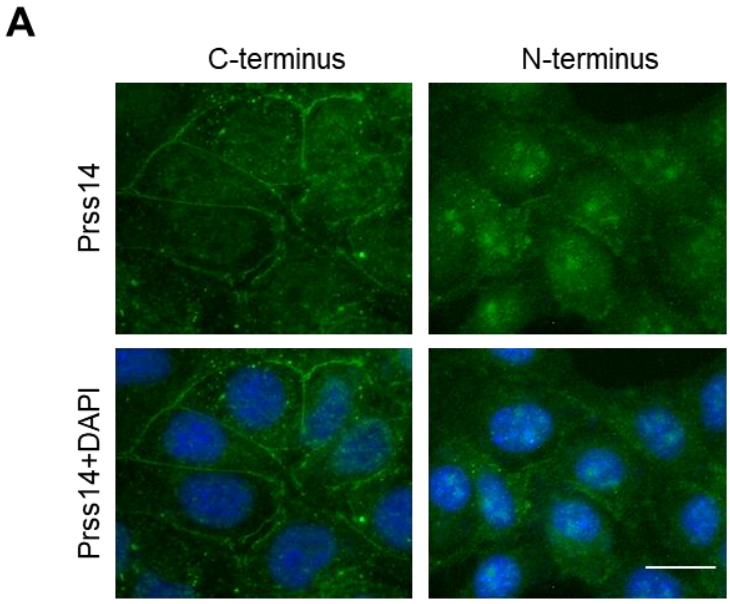
A
C-terminus
N-terminus
Prss14
Prss14+DAPI

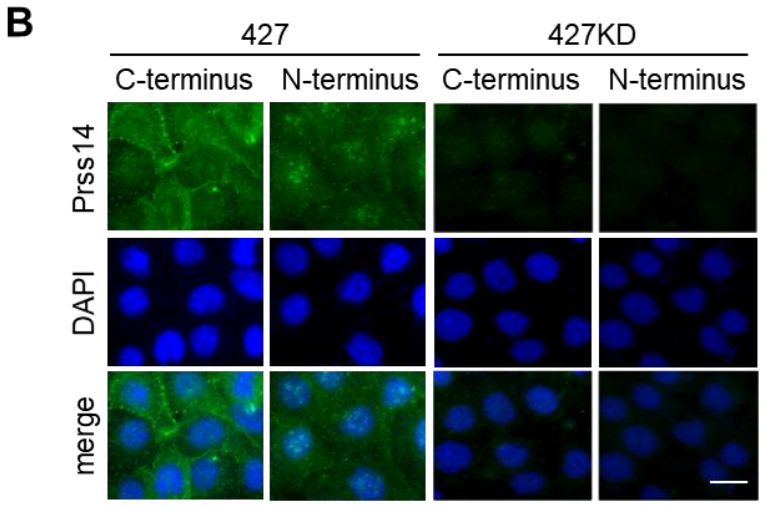
B
427
427KD
C-terminus
N-terminus
C-terminus
N-terminus
Prss14
DAPI
merge

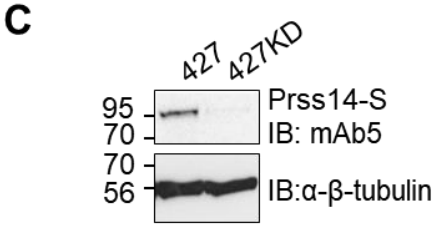
C
427
427KD
95
70
Prss14-S
IB: mAb5
70
56
IB:α-β-tubulin

Figure 5. Cellular localization of Flag-tagged Prss14 N-terminus

COS7 cells were transfected with Flag-N55 and stained with anti-Flag antibody. Localization of the Flag-tagged Prss14 N-terminus was observed. Scale bars, 20 μm.

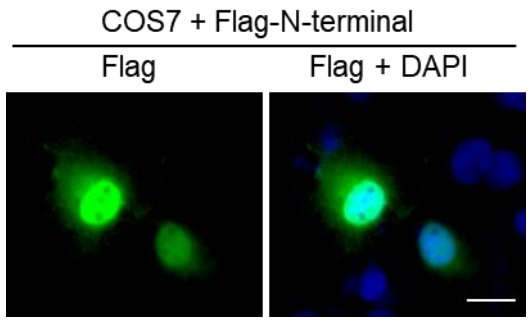
COS7 + Flag-N-terminal
Flag
Flag + DAPI

were cleaved by intramembrane proteases and generated the intracellular domain to translocate to the nucleus through RIP process (Brown et al., 2000), it was hypothesized that the nuclear staining of the Prss14 N-terminus was resulted from RIP. Prss14 is shed by various stimuli including serum (Benaud et al., 2001), PMA (Kim et al., 2005), TGF-β (Lee et al., 2014), hypoxia (Kim et al., 2010), and acidic buffer (Wang et al., 2009). Generally, RIP is proceeded by ectodomain shedding (Brown et al., 2000) and the PMA, one of the stimuli of Prss14 ectodomain shedding, was tested to be able to induce RIP.

To investigate the effect of PMA on the N-terminal fragmentation of Prss14, the localization of N-terminus was detected using anti-Prss14 N-terminus antibody (N-antibody). In PMA-treated 427.1.86 cells, the nuclear staining Prss14 was increased compared to the cells under serum deprivation (Fig. 6). Next, to verify the presence of the N-terminal fragment, western blot analysis following immunoprecipitation with N antibody was performed. PMA treatment enhances not only shed Prss14 (Prss14-S'), but also a smaller fragment with a molecular weight (~14 kDa, Fig. 7A). These results suggest that Prss14 is processed by another proteolysis called RIP and the cleaved Prss14 intracellular domain (PICD) is translocated to the nucleus.

To address whether PMA-mediated ectodomain shedding is critical for PICD generation, the shedding was inhibited and observed PICD generation. The PMA-induced ectodomain shedding of Prss14

Figure 6. PMA treatment enhances the nuclear localization of Prss14 N-terminus

427.1.86 cells were deprived serum for 2 h and treated with 1μM PMA for another 2 h. Cellular localization of Prss14 N-terminus was observed with N antibody. Scale bars, 20 μm.

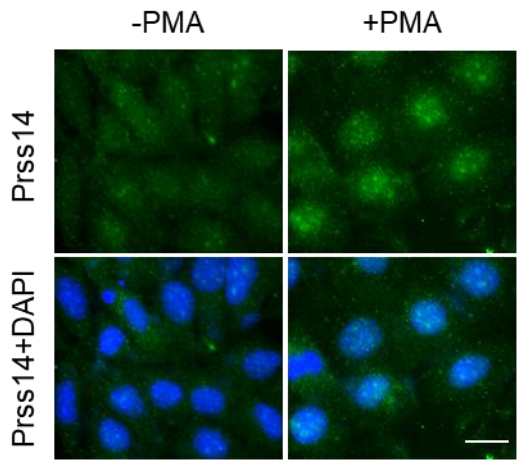
-PMA
+PMA
Prss14
Prss14+DAPI

Figure 7. PMA-induced Prss14 ectodomain shedding induces generation of the PICD

(A) Endogenous PICD detected by immunoprecipitation with anti-N antibody in 427.1.86 cells in the absence or presence of PMA. Anti-N antibody was used for western blot. (B) Western blot analysis of PICD immunoprecipitated with anti-N antibody in 427.1.86 cells treated with PMA in the absence or presence of TAPI-0.

A

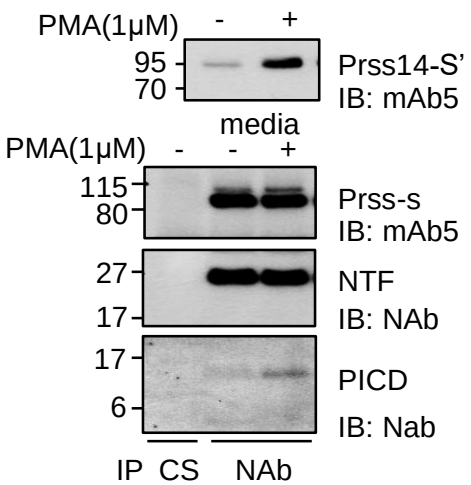
PMA(1μM) - +
95
70
Prss14-S'
IB: mAb5
media
PMA(1μM) - - +
115
80
Prss-s
IB: mAb5
27
17
NTF
IB: NAb
17
6
PICD
IB: Nab
IP CS NAb

B

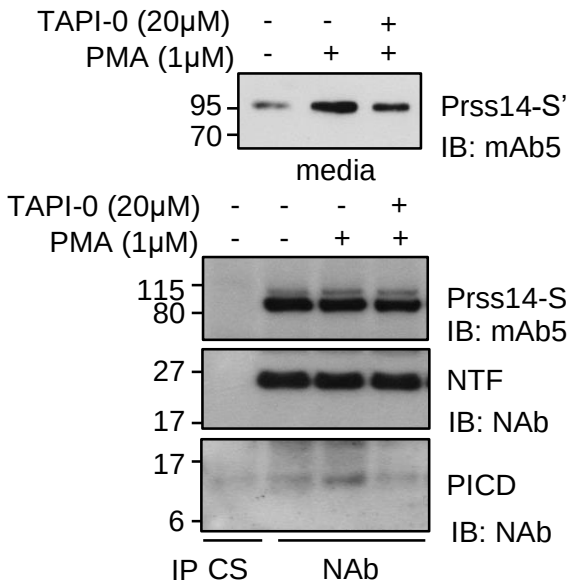
TAPI-0 (20μM) - - +
PMA (1μM) - + +
95
70
Prss14-S'
IB: mAb5
media
TAPI-0 (20μM) - - - +
PMA (1μM) - - + +
115
80
Prss14-S
IB: mAb5
27
17
NTF
IB: NAb
17
6
PICD
IB: NAb
IP CS NAb

Figure 8. PICD generation is also observed in MCF7 human breast cancer cell line

MCF7 human breast cancer cells were subjected to immunoprecipitation with anti-hN antibody against human Prss14 N-terminus. Normal rabbit serum (CS) was used for negative control. All Figures are representative of more than three independent experiments.

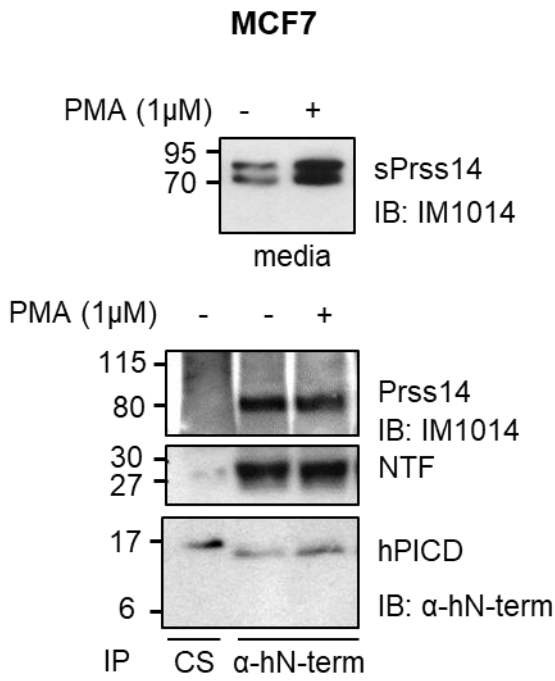
MCF7
PMA (1μM) - +
95
70
sPrss14
IB: IM1014
media
PMA (1μM) - - +
115
80
Prss14
IB: IM1014
30
27
NTF
17
6
hPICD
IB: α-hN-term
IP CS α-hN-term

is mediated by TACE (Cho et al., 2017). The TACE inhibitor, TAPI-0, reduced PMA-induced shedding and concomitantly the PICD generation (Fig. 7B). This result showed that ectodomain shedding is required and prerequisite step for EICD generation.

The PICD generation was also observed in MCF7 human breast cancer cell line. PICD that had similar molecular weight tobserved in 427.1.86 cells was increased by PMA treatment, showing that the generation of EICD was not specific phenomenon for 427.1.86 cells (Fig. 8). Taken together, these data suggest that Prss14 generates PICD in an ectodomain shedding-dependent manner.

SPPL2b is responsible for intramembrane proteolysis of Prss14 N-terminus

Among the intramembrane proteases known for RIP, SPPLs cleave type II-oriented transmembrane proteins (Fluhrer et al., 2009). It was investigated that SPPLs were involved in the cleavage of Prss14, a type II transmembrane protein. When sequences containing the transmembrane domain and about twenty residues before and after the transmembrane domain of Prss14 and known SPPLs' substrates, there were some conserved residues, leucines and glycine in the transmembrane domain (Fig. 9A). In addition, the SPPLs-specific inhibitor, $(Z-LL)_2$ketone, reduced the amount of PICD in PMA-stimulated cells without change in Prss14 shedding (Fig. 9B).

Figure 9. SPPLs are involved in the cleavage of Prss14

(A) Sequence alignment of regions containing predicted transmembrane domains of Prss14 and other known SPPL substrates. (B) 427.1.86 cells were treated with PMA in the absence or presence of SPPLs inhibitor, $(Z-LL)_2$ketone and subjected to immunoprecipitated with anti-N antibody. Normal rabbit serum (CS) was used for negative control.

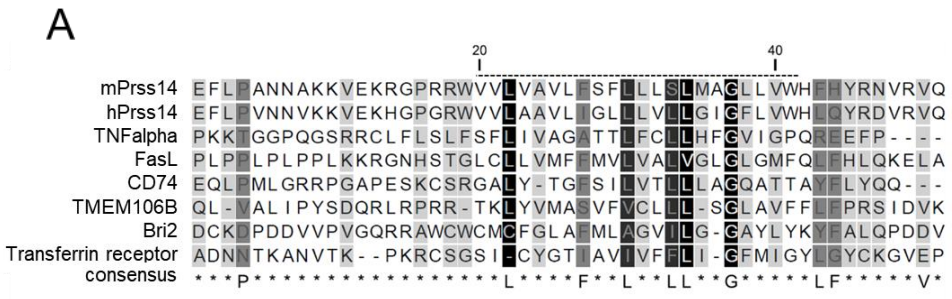
A
20
40
mPrss14 EFLPANNAKKVEKRGPRRWVVLVAVLFSFLLLSLMACLLVWHFHYRNVRVQ
hPrss14 EFLPVNNVKKVEKHGPGRWVVLAAVLIGLLLVLLGICFLVWHLQYRDVRVQ
TNFalpha PKKTGGPQGSRRCLFLSLFSFLIVAGATTLFCLLHFGVIGPQREEFP----
FasL PLPPLPLPPLKKRGNHSTGLCLLVMFFMVLVALVGLGLGMFQLFHLQKELA
CD74 EQLPMLGRRPGAPESKCSRGALY-TGFSILVTLLLAGQATTAYFLYQQ---
TMEM106B QL-VALIPYSDQRLRPRR-TKLYVMASVFVCLLL-SGLAVFFLFPRSIDVK
Bri2 DCKDPDDVVPVGQRRAWCWCMCFGLAFMLAGVILG-GAYLYKYFALQPDDV
Transferrin receptor ADNNTKANVTK--PKRCSGSI-CYGTIAVIVFFLI-GFMIGYLGYCKGVEP
consensus ***P**********L****F**L**LL**G*****LF*****V*

B

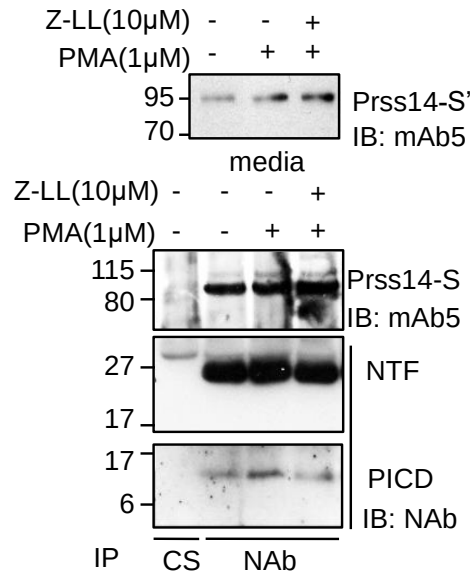
Z-LL(10μM) - - +
PMA(1μM) - + +
95
70
Prss14-S'
IB: mAb5
media
Z-LL(10μM) - - - +
PMA(1μM) - - + +
115
80
Prss14-S
IB: mAb5
27
17
NTF
17
6
PICD
IB: NAb
IP
CS
NAb

Figure 10. SPPL2b is localized at the plasma membrane

CHO-K1 cells were transiently transfected with SPPL2b-HA and localization of SPPL2b was analyzed with anti-HA antibody.

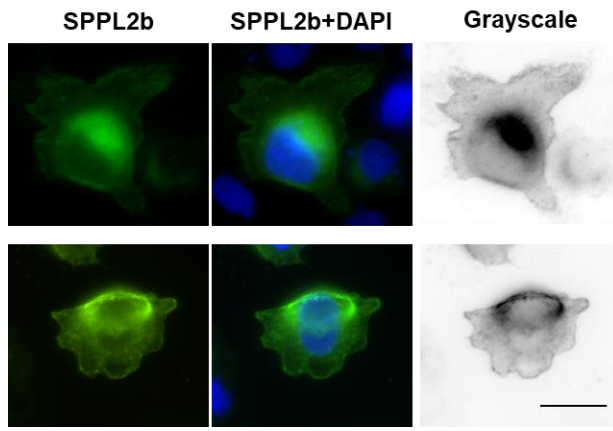
SPPL2b
SPPL2b+DAPI
Grayscale

Figure 11. Knockdown of SPPL2b reduces nuclear localization of PICD

(A) mRNA level of SPPL2b in SPPL2b-knockdown cell lines (SP2bKD-10 and -16) was detected by real time-PCR. The relative values were normalized to GAPDH signals as shown in the graphs. (B) Prss14 was stained with two kinds of anti-Prss14 antibodies in control CONT and SP2bKD-10 cells. Arrow indicates nuclear localization of PICD and arrow head indicates decreased nuclear PICD in SP2bKD-10 cells. Scale bars, 20 μm.

.

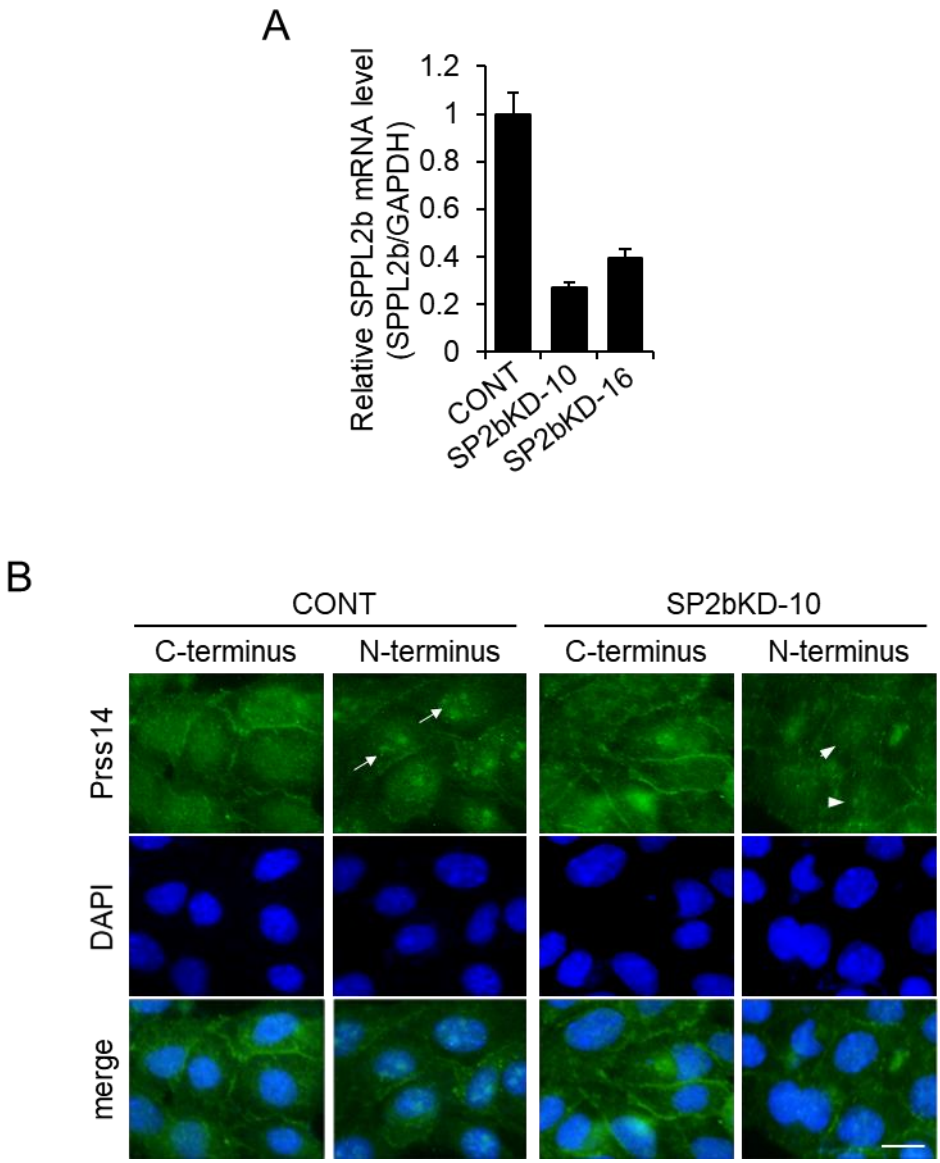
A
Relative SPPL2b mRNA level
(SPPL2b/GAPDH)
1.2
1
0.8
0.6
0.4
0.2
0
CONT
SP2bKD-10
SP2bKD-16
B
CONT
SP2bKD-10
C-terminus
N-terminus
C-terminus
N-terminus
Prss14
DAPI
merge

Figure 12. PICD generation is reduced in SPPL2b-knockdown cells even in PMA treatment

PICD was immunoprecipitated in SP2bKD cells and analyzed by Western blot with anti-N antibody with or without PMA treatment.

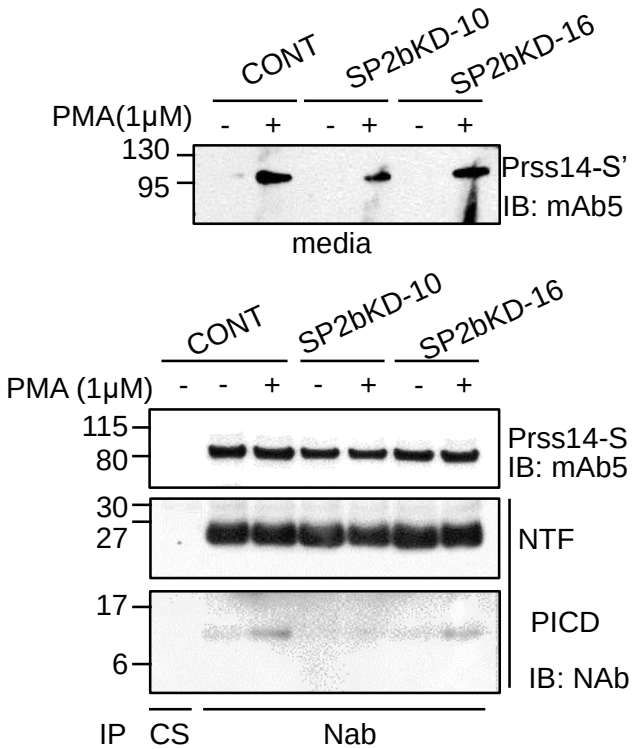
CONT
SP2bKD-10
SP2bKD-16
PMA(1μM)
- + - + - +
130
95
Prss14-S'
IB: mAb5
media
CONT
SP2bKD-10
SP2bKD-16
PMA (1μM) - - + - + - +
115
80
Prss14-S
IB: mAb5
30
27
NTF
17
6
PICD
IB: NAb
IP CS Nab

Next, I investigated which SPPL member was responsible for PICD generation. SPPL members have different cellular localization and only SPPL2b is found in the plasma membrane (Friedmann et al., 2006). Because the PICD was generated following ectodomain shedding on the cell surface, it was speculated that the plasma membrane was the place occurring RIP and SPPL2b might be the protease to cleave Prss14 NTF. As expected, SPPL2b localized at the plasma membrane in CHO-K1 cells transfected with HA-tagged SPPL2b (Fig. 10). To test that the SPPL2b is involved in generation of PICD, the nuclear localization of PICD was observed in SPPL2b-knockdown 427.1.86 cells (SP2bKD). The reduced mRNA level of SPPL2b in SP2bKD cells was shown in Fig. 11A. Nuclear localization of PICD was significantly diminished in SP2bKD cells, however, membrane localization of C-terminus was still observed in these cells (Fig. 11B). In addition, PICD was decreased compared to control cells even though PMA-induced ectodomain shedding normally occurred in these cells (Fig. 12)

To further confirm that SPPL2b indeed cleaves Prss14, SPPL2b and Prss14 were co-transfected in HEK293T cells. The expression of SPPL2b increased the amount of PICD in a dose-dependent manner in HEK293T cells (Fig. 13). These results directly indicate that SPPL2b cleaves Prss14.

To understand the relationship between ectodomain shedding and SPPL2b-mediated cleavage, we expressed Flag-tagged wild-type and truncated Prss14, Flag-N55, N149, N162, and N213 in

HEK293T cells (Fig. 14A). Cells expressing Flag-WT and Flag-N213, containing more amino acid sequences than shedding cleavage positions, generated more PICD than Flag-N149- and Flag-N162-expressing cells (Fig. 14B), suggesting that intramembrane cleavage of Prss14 by SPPL2b is tightly coupled to ectodomain shedding event. As shown in Fig. 9A, there are conserved residues between substrates of SPPLs. I-TASSER server predicted that the structure of transmembrane domain of Prss14 adopted the α-helical conformation in which peptide bonds were hard to access by proteases. It has been shown that the helix-destabilizing residues reducing the α-helical content of transmembrane domain are required for processing by intramembrane proteases (Fluhrer et al., 2012; Lemberg and Martoglio, 2002). Based on this, we determined if the conserved residues, Gly73 functioned as helix breaker for intramembrane cleavage by SPPL2b using Prss14 mutants with replacement of Gly73 to Ala (G73A). The PICD level was considerably reduced when the G73A mutant was co-expressed with SPPL2b (Fig 15), demonstrating that Gly73 is important for intramembrane proteolysis by SPPL2b.

PICD participates in transcriptional regulation

The nuclear localization of PICD suggested a possible role in regulating gene transcription. To investigate target genes regulated by PICD, RNA-seq was performed. RNA samples were prepared

Figure 13. Expression of SPPL2b increases PICD in dose-dependent manner

Western blot analysis of PICD by Flag antibody from HEK293T cells transfected with Flag-Prss14 and increasing amounts of SPPL2b-HA. An arrowhead indicates SPPL2b. The graph shows the relative amount of PICD as fold change compared to PICD of cells transfected with 0.25 μg of Prss14. PICD band intensities were normalized to SPPL2b-HA and tubulin band. The graph is represented as the mean ± SEM from three independent experiments. Statistical analysis was performed using an unpaired two-tailed student t-test. *$p < 0.05$, **$p < 0.01$.

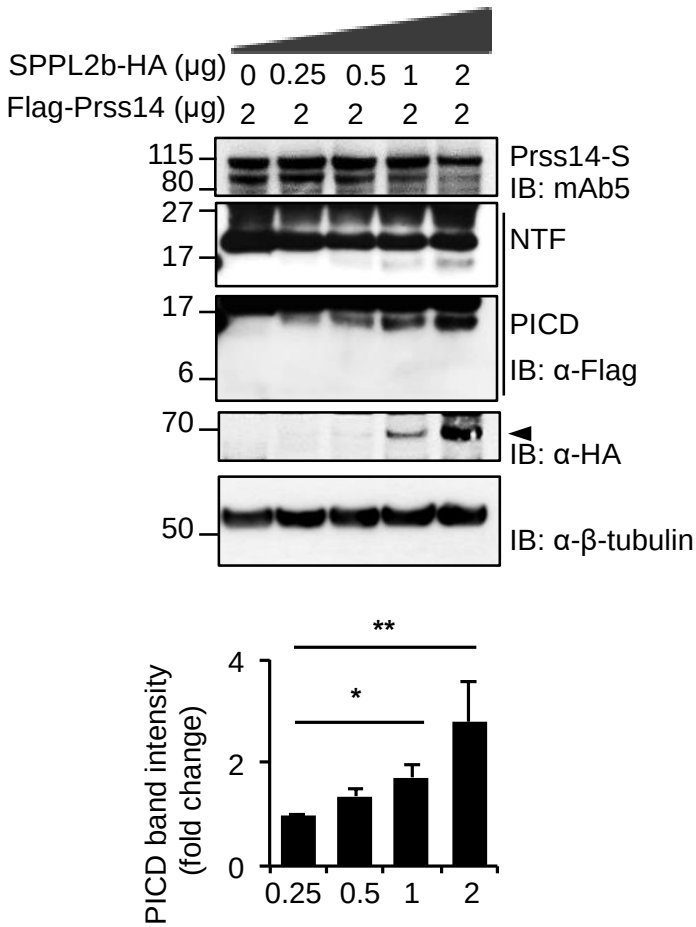
SPPL2b-HA (μg) 0 0.25 0.5 1 2
Flag-Prss14 (μg) 2 2 2 2 2
115
80
Prss14-S
IB: mAb5
27
17
NTF
17
6
PICD
IB: α-Flag
70
IB: α-HA
50
IB: α-β-tubulin
**
*
4
2
0
PICD band intensity
(fold change)
0.25 0.5 1 2

Figure 14. Ectodomain shedding is required for SPPL2b-mediated cleavage of Prss14

(A) Schematic diagrams of Prss14 domain structure and the constructs used. (B) Flag-tagged Prss14 constructs were transiently co-transfected with or without SPPL2b-HA to HEK293T cells and PICD was detected by western blot analysis. The graph shows the relative amount of PICD as fold change compared to PICD of Flag-N149. PICD band intensities were normalized to SPPL2b-HA and tubulin band. The graphs is represented as the mean ± SEM from three independent experiments. Statistical analysis was performed using an unpaired two-tailed student t-test. *$p < 0.05$, **$p < 0.01$.

A

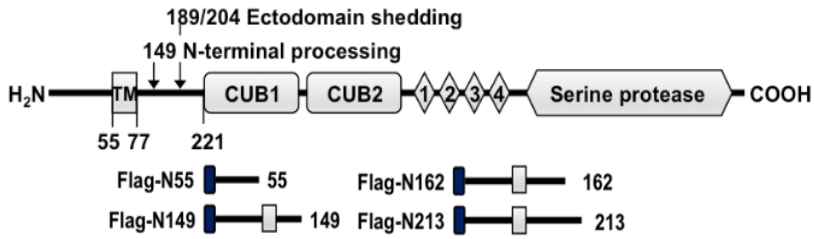
189/204 Ectodomain shedding
149 N-terminal processing
H2N
TM
CUB1
CUB2
1
2
3
4
Serine protease
COOH
55 77
221
Flag-N55
55
Flag-N162
162
Flag-N149
149
Flag-N213
213

B

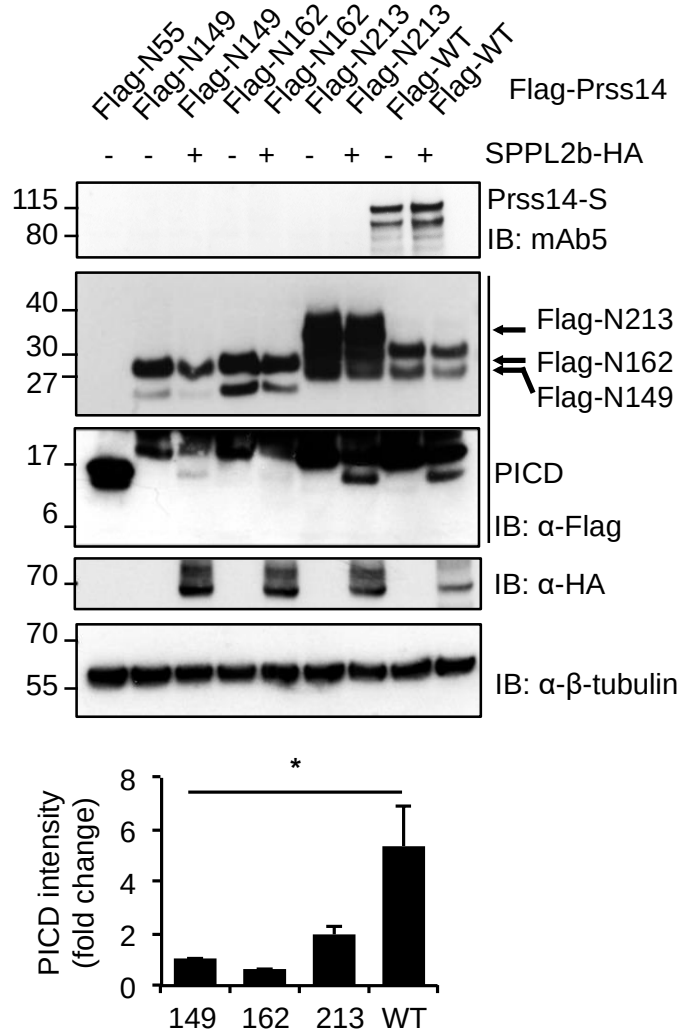
Flag-N55
Flag-N149
Flag-N149
Flag-N162
Flag-N162
Flag-N213
Flag-N213
Flag-WT
Flag-WT
Flag-Prss14
- - + - + - + - +
SPPL2b-HA
115
80
Prss14-S
IB: mAb5
40
30
27
Flag-N213
Flag-N162
Flag-N149
17
6
PICD
IB: α-Flag
70
IB: α-HA
70
55
IB: α-β-tubulin
PICD intensity (fold change)
8
6
4
2
0
*
149
162
213
WT

Figure 15. Gly73 residue is important for SPPL2b-mediated cleavage of Prss14

(A) Structure modeling of transmembrane domain of Prss14. Schematic diagrams of Prss14 domain structure and the constructs used. (B) Western blot analysis of PICD from HEK293T cells transiently co-transfected with SPPL2b-HA and Flag-Prss14 (WT) or Flag-Prss14-G73A (G73A). The graph shows the relative amount of PICD as fold change compared to PICD of wildtype. PICD band intensities were normalized to SPPL2b-HA and tubulin band. The graph is represented as the mean ± SEM from three independent experiments. Statistical analysis was performed using an unpaired two-tailed student t-test. *$p < 0.05$, **$p < 0.01$.

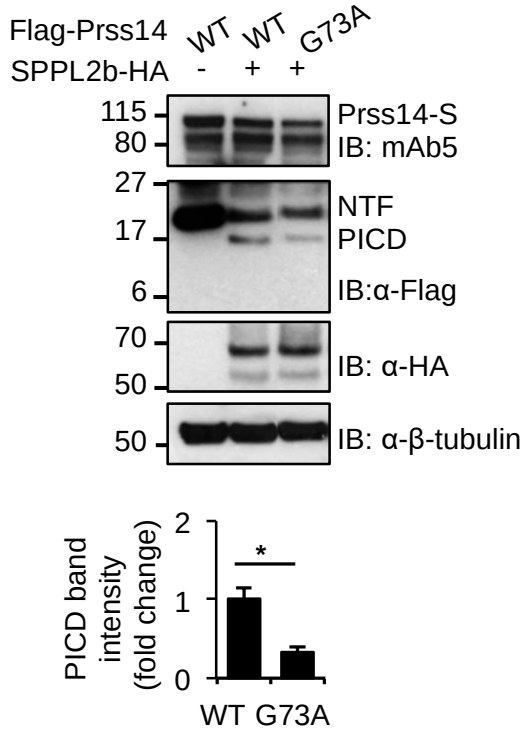
Flag-Prss14
WT
WT
G73A
SPPL2b-HA
-
+
+
115
80
Prss14-S
IB: mAb5
27
17
6
NTF
PICD
IB:α-Flag
70
50
IB: α-HA
50
IB: α-β-tubulin
PICD band intensity (fold change)
2
1
0
*
WT
G73A

Figure 16. RNA samples preparation for RNA-seq

(A) The schematic diagram describes how to prepare RNA samples for RNA-seq. (B) SP2bKD cells were transfected with GFP vector and Flag-vector or GFP vector and Flag-N55 for 24 h and GFP-positive cells were sorted.

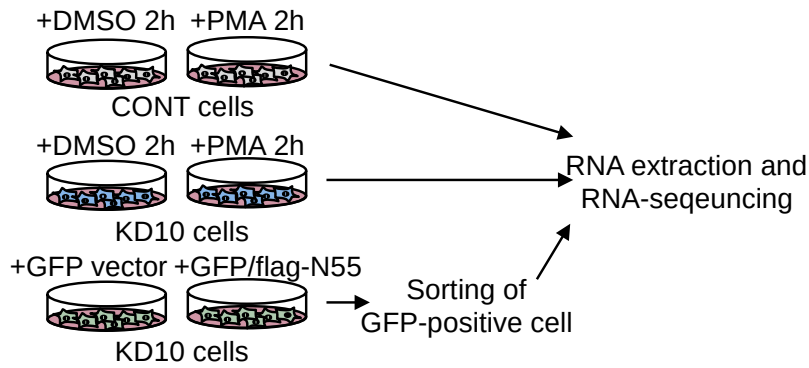
+DMSO 2h
+PMA 2h
CONT cells
+DMSO 2h
+PMA 2h
KD10 cells
+GFP vector
+GFP/flag-N55
KD10 cells
Sorting of
GFP-positive cell
RNA extraction and
RNA-seqeuncing

Figure 17. Flow chart of how to analyze the RNA-seq results

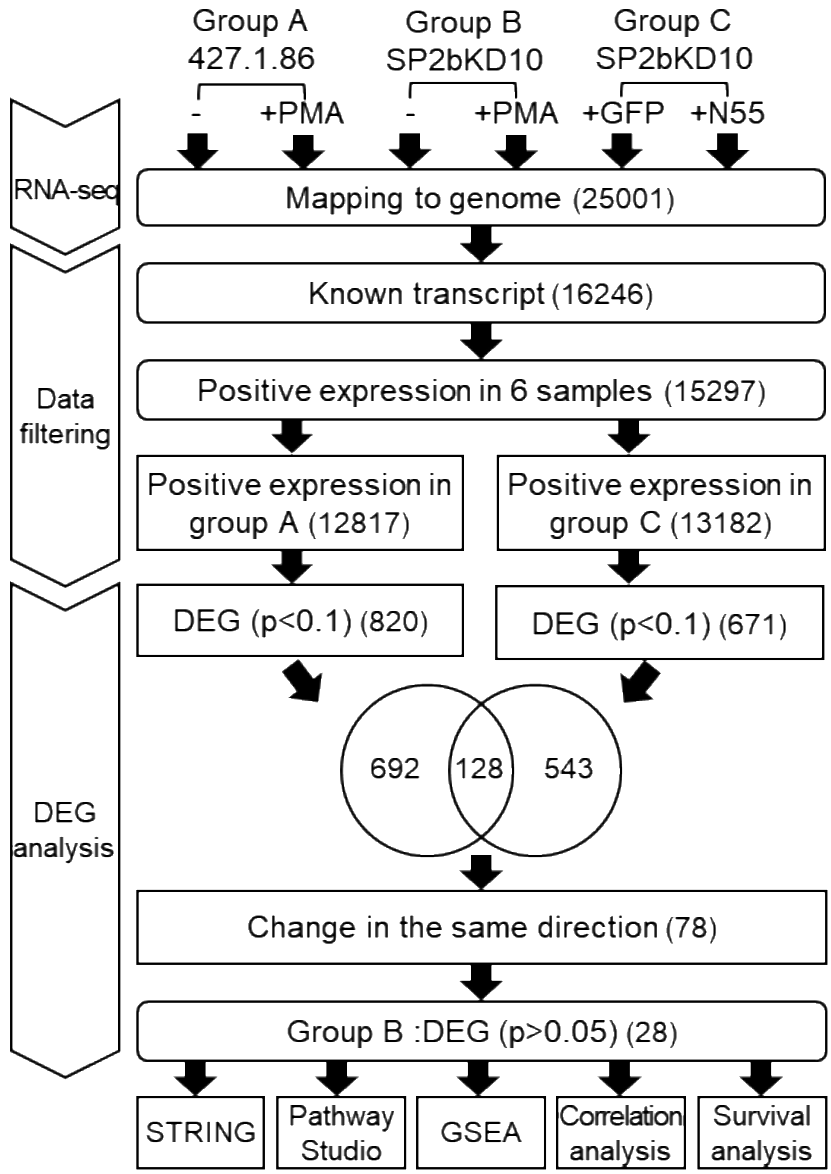
Group A
427.1.86
Group B
SP2bKD10
Group C
SP2bKD10
-
+PMA
-
+PMA
+GFP
+N55
RNA-seq
Mapping to genome (25001)
Known transcript (16246)
Data filtering
Positive expression in 6 samples (15297)
Positive expression in group A (12817)
Positive expression in group C (13182)
DEG (p<0.1) (820)
DEG (p<0.1) (671)
692
128
543
DEG analysis
Change in the same direction (78)
Group B :DEG (p>0.05) (28)
STRING
Pathway Studio
GSEA
Correlation analysis
Survival analysis

Table 1. The list of target genes regulated by PICD

Gene Symbol	Description	Cellular process				Promoter binding[$]		
		Migration[†]	Invasion[†]	EMT[‡]	TNF pathway[†]	*FOS*	*ATF3*	*RPDM1*
	Up-regulated genes							
ABCA12	ATP-binding cassette, sub-family A (ABC1) member 12			O		O		
ANKRD22	ankyrin repeat domain 22					O		
ATF3	activating transcription factor 3	O	O	O	O	O	O	O
CEACAM19	carcinoembryonic antigen-related cell adhesion molecule 19							
CXCL2	chemokine (C-X-C motif) ligand 2	O	O		O	O	O	O
CXCL3	chemokine (C-X-C motif) ligand 3	O			O			
DAGLA	diacylglycerol lipase, alpha					O	O	
EFEMP2	epidermal growth factor-containing fibulin-like extracellular matrix protein 2	O	O	O		O	O	
EGR2	early growth response 2				O	O	O	
EGR3	early growth response 3			O	O			
FOS	FBJ osteosarcoma oncogene	O	O	O	O	O	O	
FOXO1	forkhead box O1			O		O		
HIVEP3	human immunodeficiency virus type I enhancer binding protein 3					O		
LHFPL2	lipoma HMGIC fusion partner-like 2					O		
LONRF1	LON peptidase N-terminal domain and ring finger 1					O	O	
MMP13	matrix metallopeptidase 13	O	O	O	O	O		
NABP1	nucleic acid binding protein 1					O	O	
NR4A1	nuclear receptor subfamily 4, group A, member 1	O	O	O	O	O		
PRDM1	PR domain containing 1, with ZNF domain	O	O		O	O		
RND1	Rho family GTPase 1	O	O	O		O	O	
SAT1	spermidine/spermine N1-acetyl transferase 1	O	O	O	O	O	O	
STK40	serine/threonine kinase 40					O	O	
TNF	tumor necrosis factor	O	O	O	O	O		
TNFRSF1B	tumor necrosis factor receptor superfamily, member 1b				O	O		
TNFSF15	tumor necrosis factor (ligand) superfamily, member 15	O	O			O	O	O
USP43	ubiquitin specific peptidase 43					O		
VGF	VGF nerve growth factor inducible			O		O	O	
	Down-regulated genes							
UBC	Ubiquitin C						O	O

Gene symbols in bold encode transcription factors
Cellular process that each gene is involved was analyzed by Pathway Studio[†] and literature search[‡]
[$] *FOS, ATF3*, or *PRDM1* results were drived from CHIPseq in Encode database

Table 2. The list of publication showing causative roles for EMT

Gene Symbol	EMT	Reference
ABCA12	O	(Kan et al., 2012)
ANKRD22		
ATF3	O	(Yin et al., 2010)
CEACAM19		
CXCL2		
CXCL3		
DAGLA		
EFEMP2	O	(Zhang et al., 2017)
EGR2		
EGR3	O	(Chaudhury et al., 2016)
FOS	O	(Eger et al., 2000; Gao et al., 2015; Shao et al., 2014)
FOXO1	O	(Dong et al., 2017)
HIVEP3		
LHFPL2		
LONRF1		
MMP13	O	(Huang et al., 2016; Shan et al., 2018)
NABP1		
NR4A1	O	(Hedrick and Safe, 2017; Zhou et al., 2014)
PRDM1		
RND1	O	(Okada et al., 2015)
SAT1	O	(Wang et al., 2017)
STK40		
TNF	O	(Chua et al., 2007; Wang et al., 2013)
TNFRSF1B		
TNFSF15		
USP43		
VGF	O	(Hwang et al., 2017)
UBC		

from three sets of conditions (Fig. 16A). First, to see the genes induced by RIP following PMA-mediated shedding, RNA from non-treated 427.1.86 cells (CONT) was compared with that from PMA-treated cells (CONT+PMA) (group A). Second, to exclude SPPL2b-independent PMA effects, RNAs from SPPL2b-knockdown cells showing reduced PICD generation (SP2bKD-10, KD) and PMA-treated SP2bKD-10 cells (KD+P) were compared (group B). Finally, to determine the direct effect of PICD, RNAs from SP2bKD-10 cells transfected with a GFP vector (KD/GFP) and those from SP2bKD-10 cells co-transfected with a GFP vector and Flag-N55 (KD/GFP+N55) were used (group C). RNAs from group C were prepared from GFP-positive sorted cells (Fig. 16B).

Fig. 17 described how I analyzed RNA-seq results to identify PICD target genes. We first filtered out genes with no expression in all 6 samples with the FPKM cutoff of 0.001 based on the expression profiles and analyzed the differentially expressed genes (DEGs). The results showed that there were 820 genes in group A and 671 genes in group C ($p < 0.1$). The 128 genes common to groups A and C were further reduced to 78 genes by considering those exhibiting the same directional changes by PMA and N55. We next removed the DEGs of group C ($p > 0.05$) to exclude SPPL2b-independent PMA effects. Finally, 28 genes that satisfied all these stringent criteria were considered as PICD target genes (Table 1).

PICD target genes are involved in cancer-associated cell processes

To investigate the functional interactions network between target genes, STRING, a web-based protein-protein association database was used. In both the mouse and human databases, the network of target genes included three subnetworks, *FOS*-, *TNF*-, and *UBC*-centered subnetworks comprised of transcription factors (*ATF3, EGR2, EGR3, FOS, FOXO1*, and *NR4A1*), cytokines (*CXCL2*, *CXCL3*, and *TNF*), and genes in the ubiquitin proteasome pathway (*LONRF1*, *UBC*, and *USP43*), respectively (Fig. 18 and Fig. 19).

Finally, we examined whether the target genes of PICD are involved in cell migration, invasion, and EMT, which are the known functions of Prss14 (Lee et al., 2010; Szabo et al., 2011; Tsai et al., 2014). By mining the publications, I found 12 genes to induce EMT (Table 2). Pathway Studio showing that target genes are associated in which cellular processes and signaling pathway presented that 11 of 28 genes were known to be involved in cell migration and invasion. PICD target genes were also involved in many cellular processes associated with cancer progression, such as immune response, cell proliferation, and angiogenesis (Table 3). Furthermore, many target genes (13 of 28) were associated in the TNF pathway that was one of the center molecules in the network (Table 1). Because 8 of the final targets are known transcription factors, we investigated if PICD induces transcriptional activation of its targets indirectly through these transcription factors. At the time of the search, ENCODE

Table 3. Top cellular processes of PICD target genes

Top cellular processes	p-value	Genes
Immune response	5.48E-08	ATF3, CXCL2, CXCL3, EGR2, EGR3, FOS, FOXO1, MMP13, NR4A1, PRDM1, SAT1, TNF, TNFRSF1B, TNFSF15
Cell proliferation	5.80E-08	ANKRD22, ATF3, CXCL2, CXCL3, DAGLA, EFEMP2, EGR2, EGR3, FOS, FOXO1, HIVEP3, MMP13, NABP1, NR4A1, PRDM1, SAT1, STK40, TNF, TNFRSF1B, TNFSF15, UBC, VGF
Cell survival	1.24E-07	ATF3, CXCL2, CXCL3, EGR2, FOS, FOXO1, HIVEP3, MMP13, NR4A1, PRDM1, SAT1, TNF, TNFRSF1B, TNFSF15, VGF
Cell invasion	1.26E-07	ATF3, CXCL2, EFEMP2, EGR3, FOS, FOXO1, MMP13, NR4A1, PRDM1, RND1, SAT1, TNF, TNFRSF1B, TNFSF15
Tumor growth	1.75E-07	ANKRD22, ATF3, CXCL2, CXCL3, EFEMP2, EGR3, FOS, FOXO1, MMP13, NR4A1, PRDM1, SAT1, TNF, TNFRSF1B, TNFSF15
Cell migration	2.11E-07	ATF3, CXCL2, CXCL3, EFEMP2, EGR2, EGR3, FOS, FOXO1, MMP13, NR4A1, PRDM1, RND1, SAT1, TNF, TNFRSF1B, TNFSF15
Angiogenesis	2.60E-07	ATF3, CXCL2, CXCL3, EFEMP2, EGR2, EGR3, FOS, FOXO1, MMP13, NR4A1, TNF, TNFRSF1B, TNFSF15
Cell growth	2.65E-07	ATF3, CXCL2, CXCL3, EFEMP2, EGR2, EGR3, FOS, FOXO1, HIVEP3, MMP13, NR4A1, PRDM1, RND1, SAT1, TNF, TNFRSF1B, TNFSF15, UBC,
Cell differentiation	8.15E-07	ABCA12, ATF3, CXCL2, CXCL3, EFEMP2, EGR2, EGR3, FOS, FOXO1, HIVEP3, MMP13, NR4A1, PRDM1, SAT1, STK40, TNF, TNFRSF1B, TNFSF15,
Regulation of apoptosis	2.12E-06	ANKRD22, ATF3, CXCL2, CXCL3, EFEMP2, EGR2, EGR3, FOS, FOXO1, HIVEP3, MMP13, NR4A1, PRDM1, SAT1, STK40, TNF, TNFRSF1B, TNFSF15, UBC,

Figure 18. Network analysis of PICD target genes with mouse database

Network analysis of 28 PICD target genes using STRING with mouse database. Genes with no links are not presented. Interactions are represented as edges.

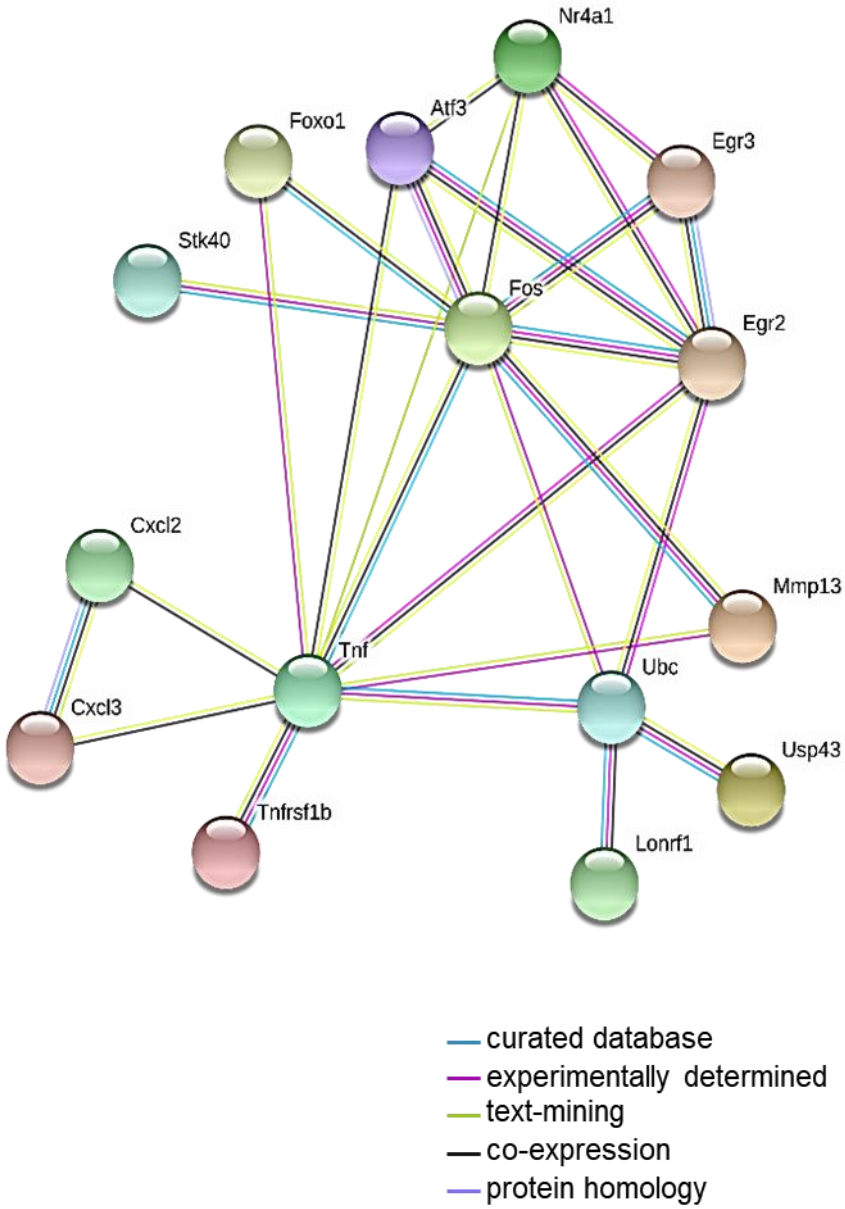
Nr4a1
Atf3
Foxo1
Egr3
Stk40
Fos
Egr2
Cxcl2
Mmp13
Tnf
Ubc
Cxcl3
Usp43
Tnfrsf1b
Lonrf1
curated database
experimentally determined
text-mining
co-expression
protein homology

Figure 19. Network analysis of PICD target genes with human database

Network analysis of 28 PICD target genes using STRING with human database. Genes with no links are not presented. Interactions are represented as edges.

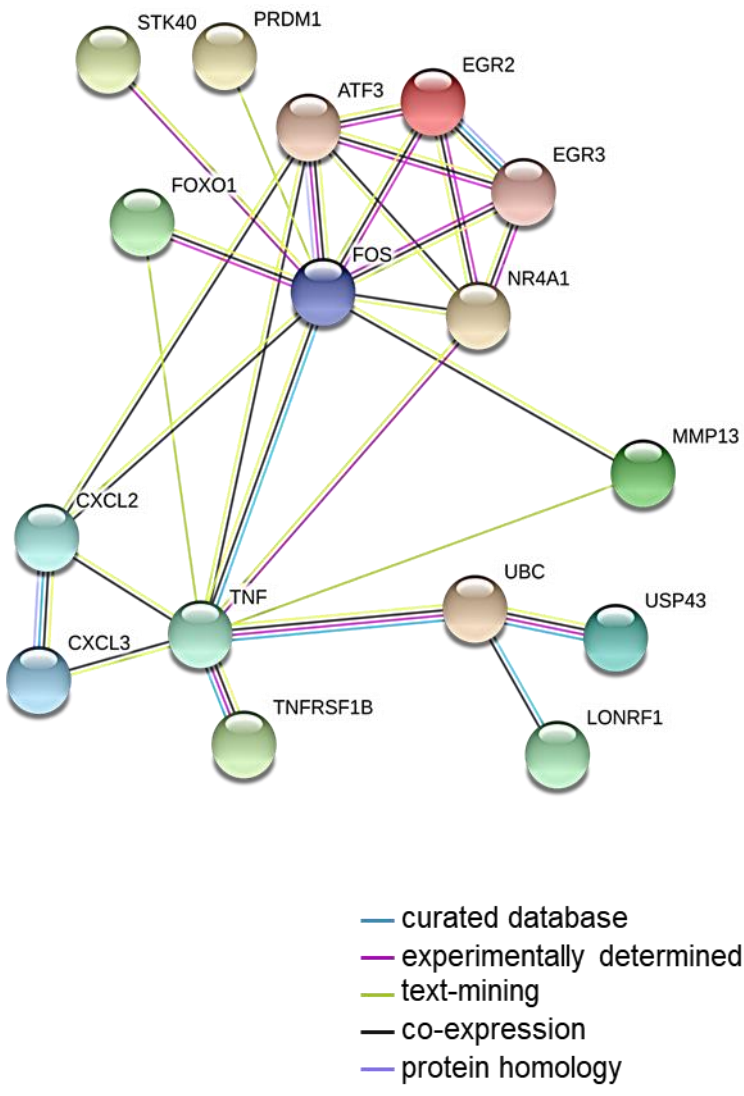
STK40
PRDM1
EGR2
ATF3
EGR3
FOXO1
FOS
NR4A1
MMP13
CXCL2
UBC
TNF
USP43
CXCL3
TNFRSF1B
LONRF1
curated database
experimentally determined
text-mining
co-expression
protein homology

(Consortium, 2012) provided information for only three transcription factors, *ATF3*, *FOS*, and *PRDM1*. ENCODE analysis showed that 24 of PICD target genes contained the binding sites for *FOS* (Table 1). Additionally, 14 targets contain *ATF3* and 4 targets contain *PRDM1* binding sites (Table 1). PICD may induce transcriptional activation of specific transcription factors, which in turn regulates the expression of genes involved in cell migration, invasion, EMT, and TNF-related pathways.

PICD is sufficient to enhance cell migration, invasion, and EMT

To validate the computational analysis showing the potential roles of PICD, we tested if PICD promotes cell migration and invasion using PICD-overexpressing 427.1.86 cells (Flag-N55-1 and -5, Fig. 20A). We found that Flag-N55 overexpression promoted cell migration ability by up to 3-fold comparing to in the control group in the wound healing assay (Fig. 21). Additionally, overexpression of Flag-N55 significantly enhanced cell invasion through Matrigel (Fig. 22). These results indicate that PICD itself is sufficient to promote migration and invasion. Although SP2bKD cells lost the ability to induce migration upon PMA stimulation, expression of Flag-N55 recovered the migration ability even without PMA stimulation (Fig. 20B and Fig. 23). PMA-induced invasion through Matrigel was abolished in SP2bKD cells, but this impaired cell invasion was rescued by Flag-N55 expression (Fig. 24). Flag-N55 cells showed

Figure 20. Flag-N55 is stably transfected in 427.1.86 cells and transiently expressed in SP2bKD-10 cells

(A) Western blot analysis of 427.1.86-Flag-N55 cell lines with anti-Flag antibody. (B) SP2bKD-10 cells were transiently transfected with Flag-N55. After 24 h of transfection, expression of Flag-N55 was analyzed by Western blotting with anti-Flag antibody. Tubulin was used as a loading control.

A

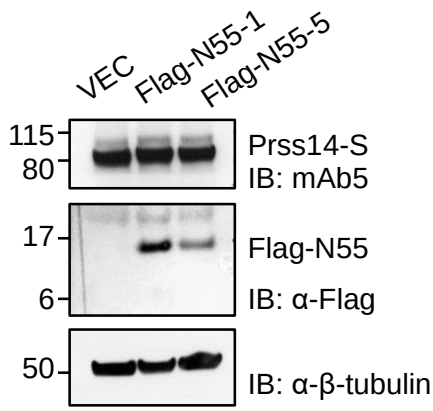
VEC
Flag-N55-1
Flag-N55-5
115
80
Prss14-S
IB: mAb5
17
6
Flag-N55
IB: α-Flag
50
IB: α-β-tubulin

B

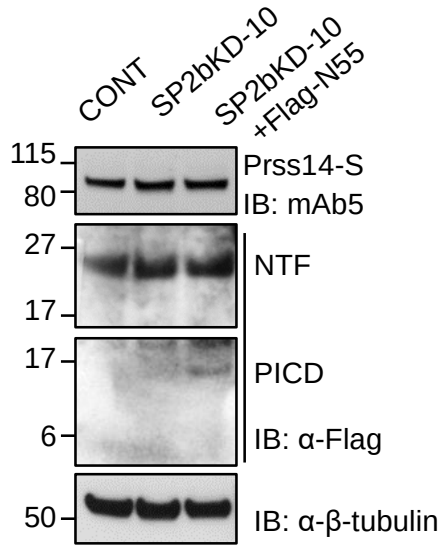
CONT
SP2bKD-10
SP2bKD-10
+Flag-N55
115
80
Prss14-S
IB: mAb5
27
17
NTF
17
6
PICD
IB: α-Flag
50
IB: α-β-tubulin

Figure 21. Cell migration is increased in Flag-N55-overexpressing cell

Wound healing assay using 427.1.86 cells stably expressing Flag-N55. Representative brightfield images at the time of 0 h and 24 h were shown. Graph shows the recovered area by migrated cells for 24 h. Cells in six different microscopic fields were examined from three independent experiments. Data are presented as a mean ± SEM (error bars). Statistical analysis was performed using an unpaired two-tailed student t-test. *$p < 0.05$, **$p < 0.01$, ***$p < 0.001$, ****$p < 0.0001$.

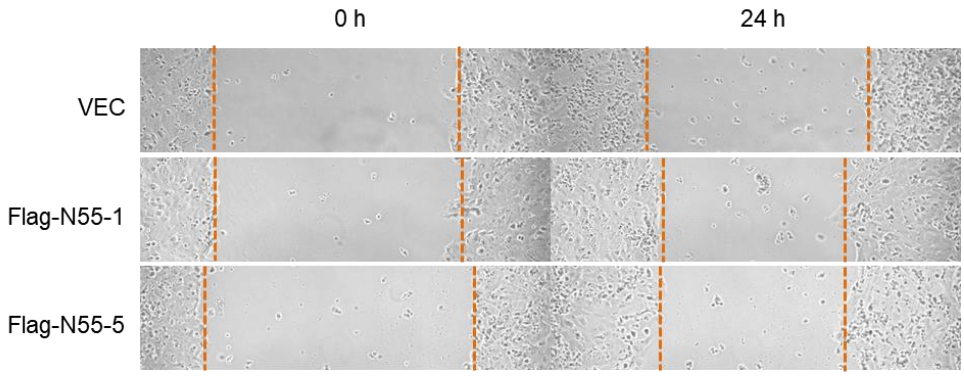
0 h
24 h
VEC
Flag-N55-1
Flag-N55-5

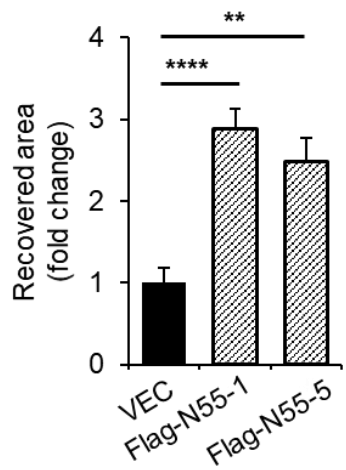
**
****
Recovered area
(fold change)
4
3
2
1
0
VEC
Flag-N55-1
Flag-N55-5

Figure 22. Cell invasion is increased in Flag-N55-overexpressing cell

Invasive activity of Flag-N55 expressing cells was investigated using Matrigel invasion assay. Representative brightfield images of invaded cells were shown. Graph shows migrated cells to the outer chamber for 24 h. Cells in fifteen different microscopic fields were examined from three independent experiments. Data are presented as a mean ± SEM (error bars). Statistical analysis was performed using an unpaired two-tailed student t-test. *p < 0.05, **p < 0.01, ***p < 0.001, ****p < 0.0001.

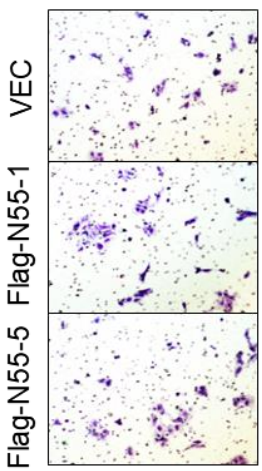
VEC
Flag-N55-1
Flag-N55-5

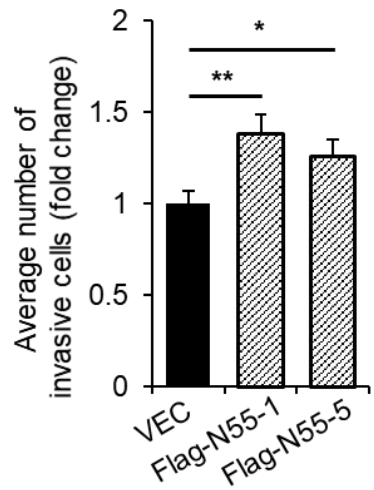
Average number of invasive cells (fold change)
2
1.5
1
0.5
0
*
**
VEC
Flag-N55-1
Flag-N55-5

Figure 23. PICD generation by SPPL2b is required for cell migration

Wound healing assay using SP2bKD cells. Representative brightfield images at the time of 0 h and 24 h were shown. Graph shows the recovered area by migrated cells for 24 h in the presence or absence of PMA. Flag-N55 was transiently transfected for 24 h and used for wound healing assay. Graph shows the recovered area by migrated cells for 24 h. Cells in six different microscopic fields were examined from three independent experiments. Data are presented as a mean ± SEM (error bars). Statistical analysis was performed using an unpaired two-tailed student t-test. *$p < 0.05$, **$p < 0.01$, ***$p < 0.001$, ****$p < 0.0001$.

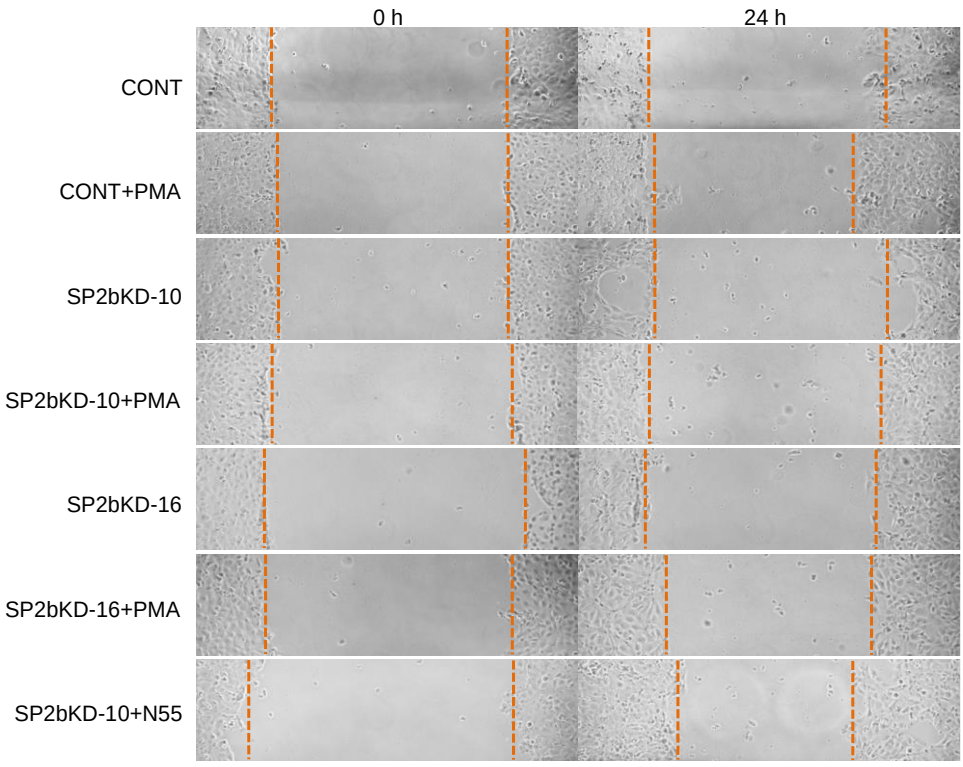
0 h
24 h
CONT
CONT+PMA
SP2bKD-10
SP2bKD-10+PMA
SP2bKD-16
SP2bKD-16+PMA
SP2bKD-10+N55

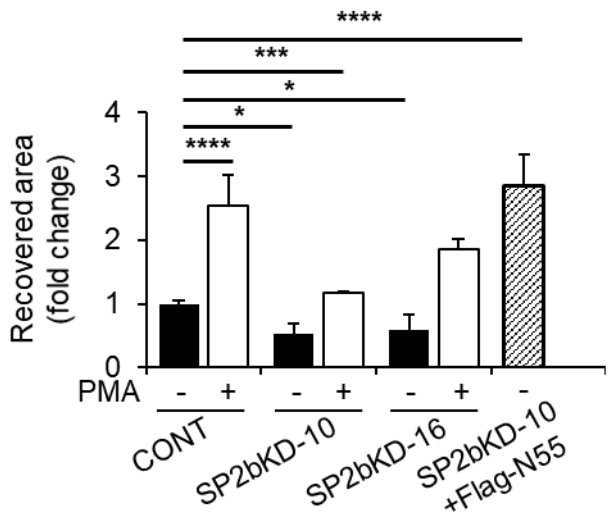
****
***
*
*
****
Recovered area
(fold change)
4
3
2
1
0
PMA
-
+
-
+
-
+
-
CONT
SP2bKD-10
SP2bKD-16
SP2bKD-10
+Flag-N55

Figure 24. PICD generation by SPPL2b is required for cell invasion

(A) Invasive activity of SP2bKD cells was measured using Matrigel invasion assay. Representative brightfield images of invaded cells were shown. Graph shows migrated cells to the outer chamber for 24 h in the presence or absence of PMA. (B) SP2bKD-10 cells were transfected with Flag-N55. 24 h after transfection, Matrigel invasion assay was performed. Cells in fifteen different microscopic fields were examined from three independent experiments. All data are presented as a mean ± SEM (error bars). Statistical analysis was performed using an unpaired two-tailed student t-test. *$p < 0.05$, **$p < 0.01$, ***$p < 0.001$, ****$p < 0.0001$.

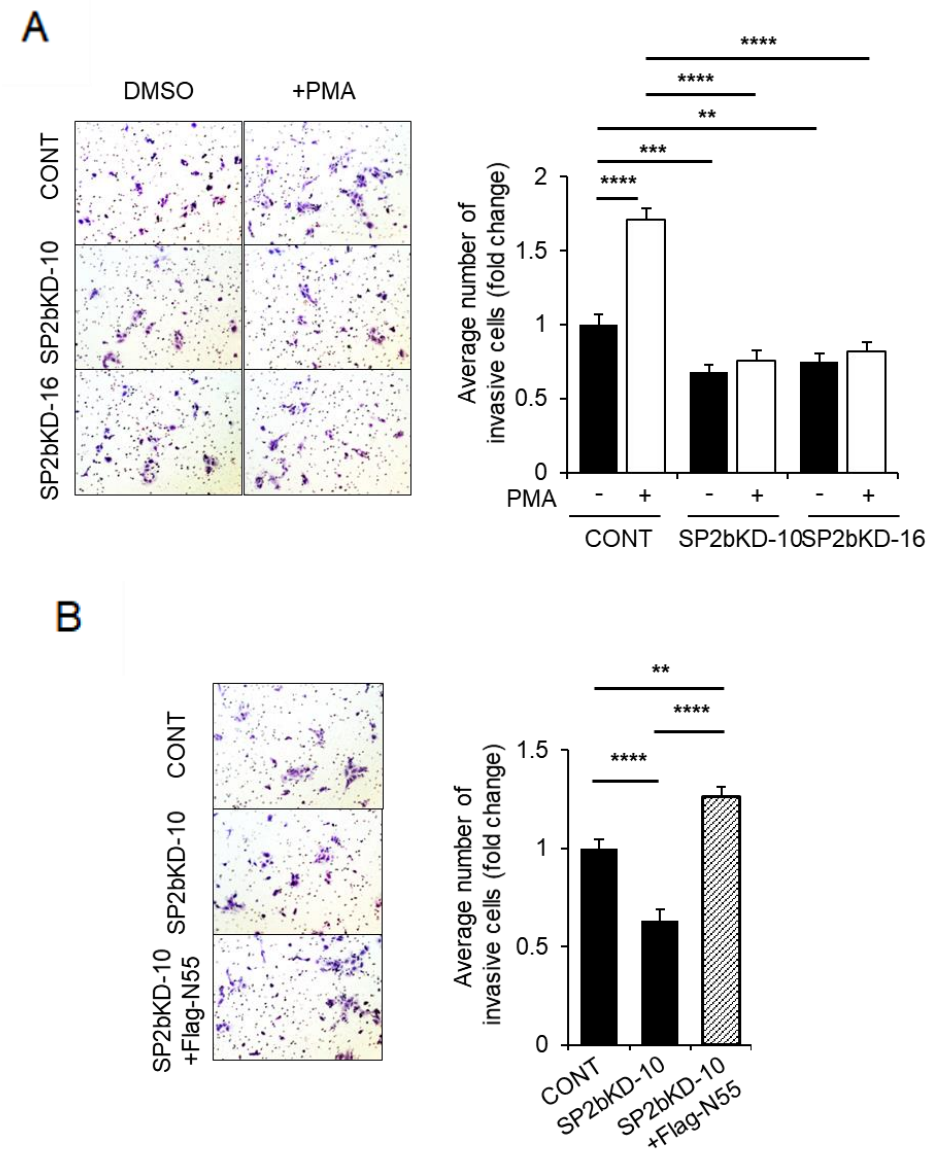
A
DMSO
+PMA
CONT
SP2bKD-10
SP2bKD-16
Average number of invasive cells (fold change)
PMA
CONT
SP2bKD-10
SP2bKD-16
B
SP2bKD-10 +Flag-N55
Average number of invasive cells (fold change)
CONT
SP2bKD-10
SP2bKD-10 +Flag-N55

Figure 25. PICD causes the morphological change

Representative brightfield images of 427.1.86 cells stably expressing Flag vector or Flag-N55. Graph shows the percentage of scattered cells over the total number of cells in each field. At least 745 cells in 50 fields were counted per condition. Scale bars, 50 μm. Data are presented as a mean ± SEM (error bars). Statistical analysis was performed using an unpaired two-tailed student t-test. *p < 0.05, **p < 0.01, ***p < 0.001, ****p < 0.0001.

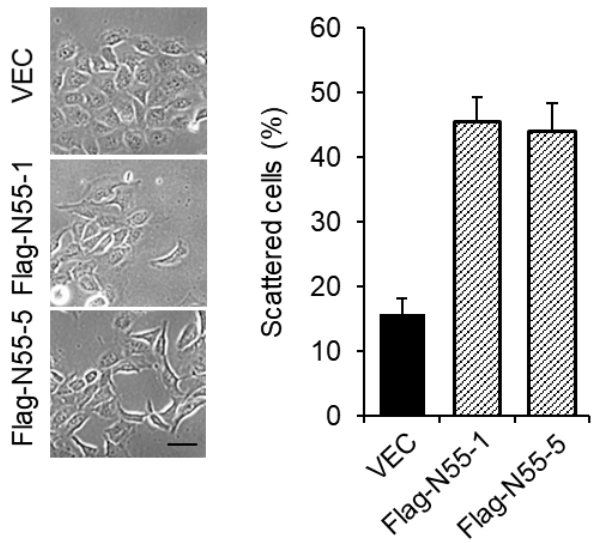
VEC
Flag-N55-1
Flag-N55-5
Scattered cells (%)
60
50
40
30
20
10
0
VEC
Flag-N55-1
Flag-N55-5

Figure 26. PICD induces the expressional changes of EMT markers

Representative immunofluorescent images of Flag-N55 cells stained for EMT markers including E-cadherin and vimentin. Scale bars, 20 μm.

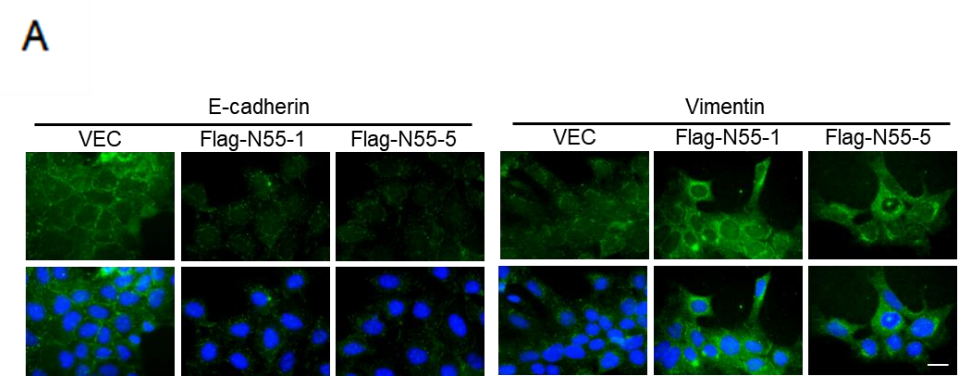
A
E-cadherin
Vimentin
VEC
Flag-N55-1
Flag-N55-5
VEC
Flag-N55-1
Flag-N55-5

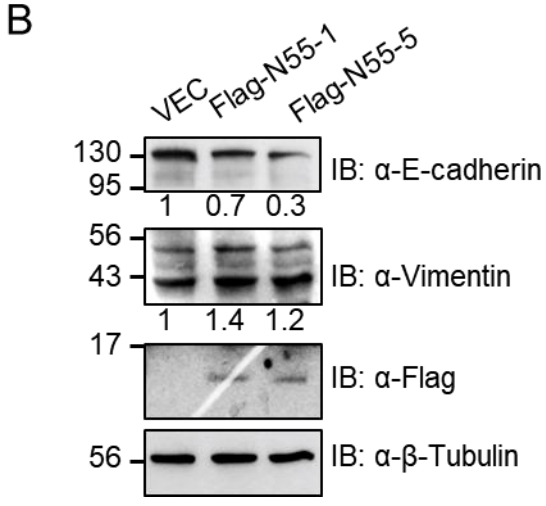
B
VEC
Flag-N55-1
Flag-N55-5
130
95
IB: α-E-cadherin
1 0.7 0.3
56
43
IB: α-Vimentin
1 1.4 1.2
17
IB: α-Flag
56
IB: α-β-Tubulin

the cellular morphology with loosened cell-cell adhesion and a more elongated and scattered phenotype compared to the cell expressing Flag vector in normal culture conditions (Fig. 25). While the epithelial marker E-cadherin was decreased in Flag-N55 cells, the mesenchymal marker vimentin was increased (Fig. 26A and Fig. 26B). Taken together, these results indicate that PICD generated by RIP plays important roles in migration, invasion, and EMT, which is consistent with the results of RNA-seq analysis.

Expression of PICD target genes correlates with expression of *PRSS14* in breast cancer patients

The Prss14 is upregulated in breast cancer patients and its upregulation is implicated in poor survival (Kang et al., 2003; Kim et al., 2016; Welm et al., 2007). Therefore, the clinical relevance of PICD-regulated genes was investigated in breast cancer patients using The Cancer Genome Atlas (TCGA). First, gene set enrichment analysis (GSEA) was performed with the PICD target gene set and TCGA breast cancer dataset separated into high and low *PRSS14* expression. The results showed that PICD target genes were significantly enriched in high *PRSS14* expression group at the stringent false discovery rate (FDR) cutoff of less than 0.05 (NES = 1.675, FDR = 0.012, Fig. 27). Next, the correlation of expression between each target gene and SPPL2B in the high PRSS14 group was analyzed to evaluate whether target genes were regulated by *SPPL2B* and *PRSS14* in breast cancer patients. When the expression

Figure 27. GSEA using PICD target genes in breast cancer patients

Enrichment plots of 28 PICD target genes according to *PRSS14* mRNA expression levels by gene set enrichment analysis (GSEA) from TCGA breast cancer dataset. NES, normalized enrichment score; FDR, false discovery rate.

PICD target gene list

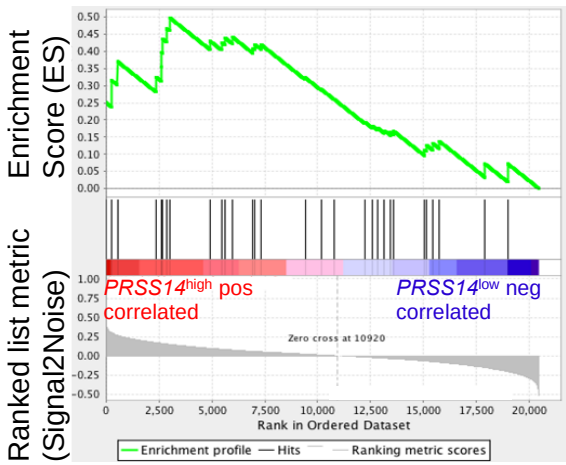

Enrichment Score (ES)	0.499
Normalized Enrichment Score (NES)	1.675
p-value	0.012
FDR	0.012

Figure 28. Correlation analysis of target gene expression with *SPPL2B* in *PRSS14*^{high} TCGA breast cancer patients

Scatter plots showing correlation between PICD target genes and *SPPL2B* in *PRSS14*^{high} TCGA breast cancer patients. r value is Correlation coefficient r values between two genes computed using Pearson correlation calculations. Two-tailed p values were calculated by an unpaired t test. *P < 0.05, ***P < 0.001,****P < 0.0001. The blue line presents the linear interpolation in whole patients.

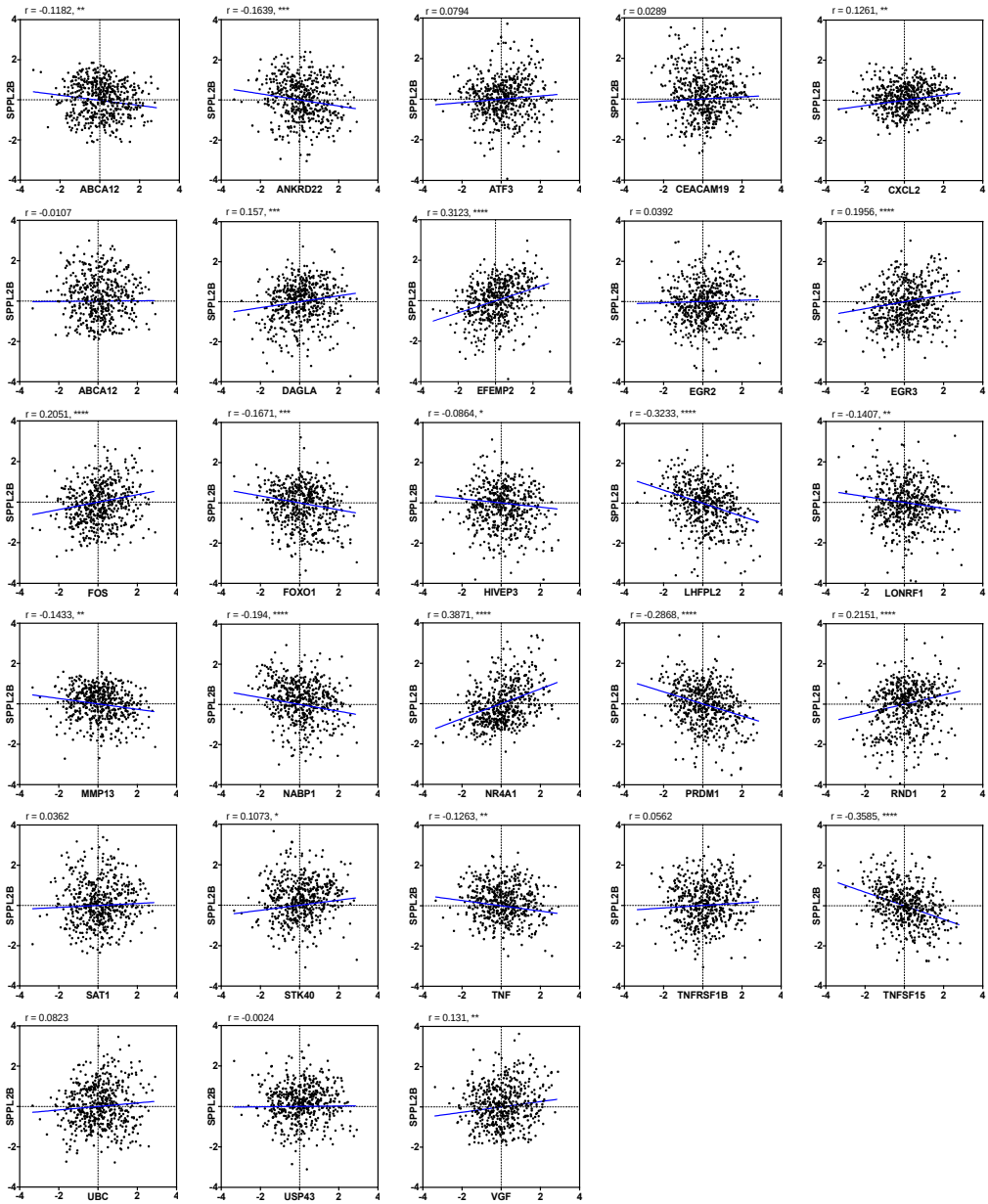
r = -0.1182, **
SPPL2B
ABCA12
r = -0.1639, ***
ANKRD22
r = 0.0794
ATF3
r = 0.0289
CEACAM19
r = 0.1261, **
CXCL2
r = -0.0107
ABCA12
r = 0.157, ***
DAGLA
r = 0.3123, ****
EFEMP2
r = 0.0392
EGR2
r = 0.1956, ****
EGR3
r = 0.2051, ****
FOS
r = -0.1671, ***
FOXO1
r = -0.0864, *
HIVEP3
r = -0.3233, ****
LHFPL2
r = -0.1407, **
LONRF1
r = -0.1433, **
MMP13
r = -0.194, ****
NABP1
r = 0.3871, ****
NR4A1
r = -0.2868, ****
PRDM1
r = 0.2151, ****
RND1
r = 0.0362
SAT1
r = 0.1073, *
STK40
r = -0.1263, **
TNF
r = 0.0562
TNFRSF1B
r = -0.3585, ****
TNFSF15
r = 0.0823
UBC
r = -0.0024
USP43
r = 0.131, **
VGF

levels of both *SPPL2B* and *PRSS14* were high, the expression of PICD generation, 9 target genes (*CXCL2, DADGLA, EFEMP2, EGF3, FOS, NR4A1, RNA1, STK40*, and *VGF*) were also high, showing a positive correlation (Fig. 28). Therefore, these results suggest that expression of these target genes is regulated by *PRSS14* and *SPPL2B* in breast cancer patients.

PICD target genes along with PRSS14 are valuable markers of ER-negative breast cancer

The *PRSS14* is the critical prognosis marker for ER negative breast cancer patients (Kim et al., 2016). I evaluated the relationship between PICD and survival of ER−negative breast cancer patients in TCGA breast cancer dataset. For this, the survival rate was analyzed according to *SPPL2B* expression which is critical factor of EICD generation. The ER−negative and $SPPL2B^{high}$ group showed the worst survival outcome (ER(−)$SPPL2B^{high}$ vs. ER(+)$SPPL2B^{low}$, hazard ratio (HR) = 3.20, $p < 0.001$, Fig. 29A). In the ER negative group, the $SPPL2B^{high}$ groups showed poorer survival than the $SPPL2B^{low}$ groups (ER(−)$SPPL2B^{high}$ vs. ER(−)$SPPL2B^{low}$, HR = 1.88, $p = 0.076$), ,indicating that high expression of *SPPL2B* determines the survival of ER−negative breast cancer patients (Fig. 29A). In the ER−negative group, the $PRSS14^{high}/SPPL2B^{high}$ group showed the poorest survival pattern, although the results were not significant, likely because of the low numbers of patient cases in this

Figure 29. Survival rate is lower in *SPPL2B*^{high} breast cancer patients than *SPPL2B*^{low}

(A) Kaplan–Meier survival analysis of four breast cancer patient groups divided by ER status and then high (hi) and low (lo) *SPPL2B* expression in total TCGA breast cancer patients. (B) ER–negative breast cancer patients were divided by expression level of *PRSS14* and *SPPL2B*. The p values were calculated using log–rank statistics. *p < 0.05, **p < 0.01, ***p < 0.001.

A

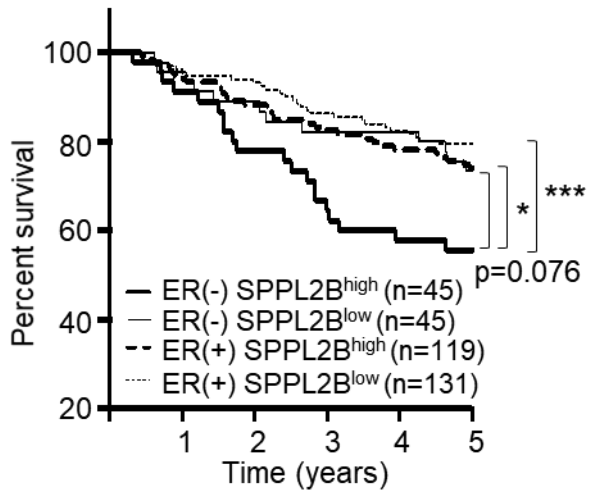
100
80
60
40
20
Percent survival
1
2
3
4
5
Time (years)
*
***
p=0.076
ER(-) SPPL2B^high (n=45)
ER(-) SPPL2B^low (n=45)
ER(+) SPPL2B^high (n=119)
ER(+) SPPL2B^low (n=131)

B

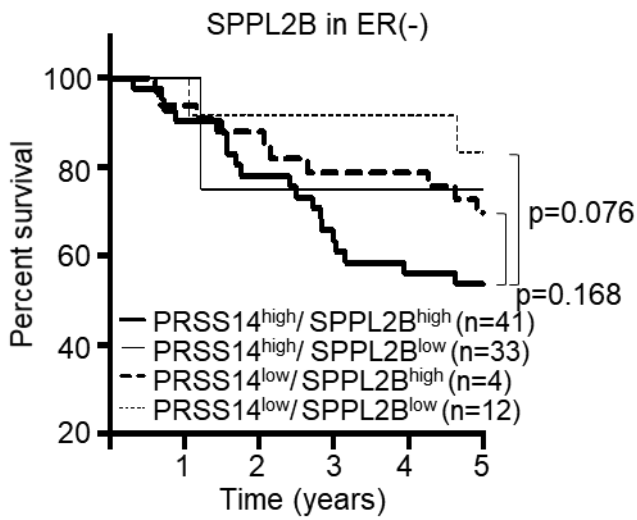
SPPL2B in ER(-)
100
80
60
40
20
Percent survival
1
2
3
4
5
Time (years)
p=0.076
p=0.168
PRSS14^high/ SPPL2B^high (n=41)
PRSS14^high/ SPPL2B^low (n=33)
PRSS14^low/ SPPL2B^high (n=4)
PRSS14^low/ SPPL2B^low (n=12)

Figure 30. ER-negative breast cancer patients with high expression of PRSS14 and PICD target genes show poorer survival

Kaplan-Meier survival analysis of ER negative patient groups divided by expression level of *PRSS14* and EPEMP2 (A), *FOS* (B), and *MMP13* (C), respectively. The p values were calculated using log-rank statistics. *p < 0.05, **p < 0.01, ***p < 0.001.

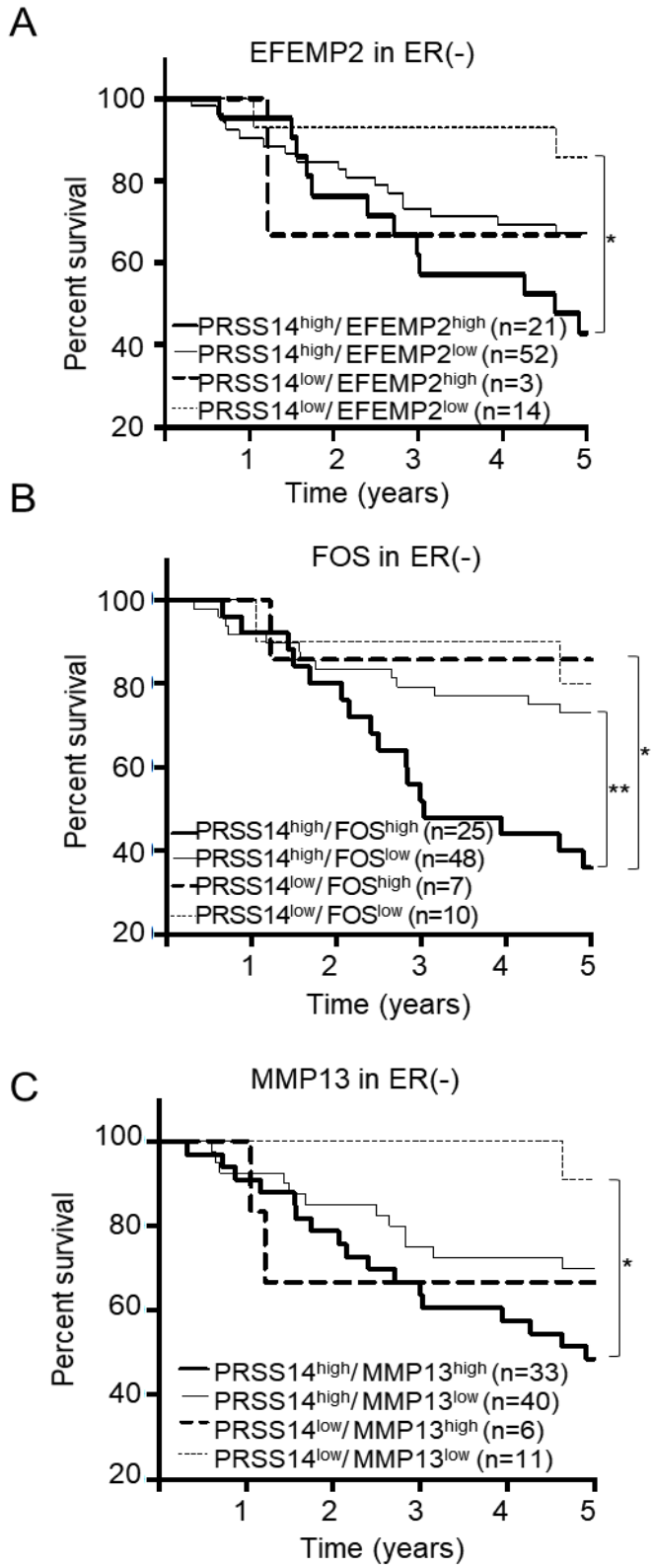
A
EFEMP2 in ER(-)
Percent survival
100
80
60
40
20
1
2
3
4
5
Time (years)
*
PRSS14high/ EFEMP2high (n=21)
PRSS14high/ EFEMP2low (n=52)
PRSS14low/ EFEMP2high (n=3)
PRSS14low/ EFEMP2low (n=14)
B
FOS in ER(-)
Percent survival
100
80
60
40
20
1
2
3
4
5
Time (years)
*
**
PRSS14high/ FOShigh (n=25)
PRSS14high/ FOSlow (n=48)
PRSS14low/ FOShigh (n=7)
PRSS14low/ FOSlow (n=10)
C
MMP13 in ER(-)
Percent survival
100
80
60
40
20
1
2
3
4
5
Time (years)
*
PRSS14high/ MMP13high (n=33)
PRSS14high/ MMP13low (n=40)
PRSS14low/ MMP13high (n=6)
PRSS14low/ MMP13low (n=11)

Figure 31. Model for PICD generation and dual function of Prss14 in cancer progression and metastasis

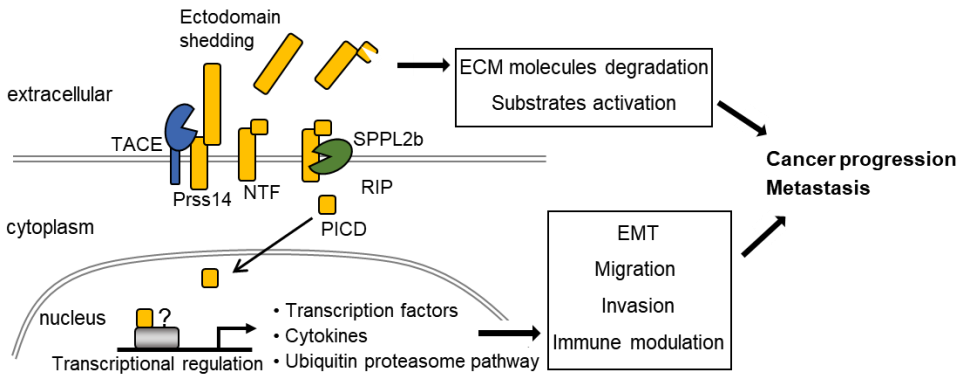
Ectodomain
shedding
extracellular
TACE
Prss14
NTF
SPPL2b
RIP
PICD
cytoplasm
nucleus
?
Transcriptional regulation
• Transcription factors
• Cytokines
• Ubiquitin proteasome pathway
ECM molecules degradation
Substrates activation
EMT
Migration
Invasion
Immune modulation
Cancer progression
Metastasis

analysis (Fig. 29B). These results suggest that expression of SPPL2B and PRSS14 are useful markers for poor prognosis in ER-negative breast cancer patients.

Survival analysis was also performed in ER negative groups divided by *PRSS14* expression and each target gene expression. Among the target genes, high expression of *FOS*, *EFEMP2*, and *MMP13* along with high *PRSS14* expression led to the worst survival. The $PRSS14^{high}/FOS^{high}$ group showed significantly worse outcomes compared to the $PRSS14^{high}/FOS^{low}$ and $PRSS14^{low}/FOS^{high}$ groups ($PRSS14^{high}/FOS^{high}$ vs. $PRSS14^{high}/FOS^{low}$, HR = 2.86, $p < 0.01$, $PRSS14^{high}/FOS^{high}$ vs. $PRSS14^{low}/FOS^{high}$, HR = 3.21, $p < 0.05$, Fig. 30A). Additionally, the $PRSS14^{high}/EFEMP2^{high}$ and $PRSS14^{high}/MMP13^{high}$ groups similarly showed the worst outcomes among the 4 groups ($PRSS14^{high}/EFEMP2^{high}$ vs. $PRSS14^{low}/EFEMP2^{low}$, HR = 2.54, $p < 0.05$ $PRSS14^{high}/MMP13^{high}$ vs. $PRSS14^{low}/MMP13^{low}$, HR = 2.90, $p < 0.05$, Fig. 30B and Fig. 30C). Therefore, a combination of *PRSS14* and *FOS*, *EFEMP2*, or *MMP13* can be used as an additional prognosis marker for ER-negative breast cancer patients.

DISCUSSION

Here, I demonstrated that the novel proteolytic processing of Prss14 by SPPL2b, which generates intracellular fragment, PICD, and its roles in regulation of gene expression involved in cancer progression. The PICD target genes are involved in cell migration, invasion, EMT, and TNF signaling pathway. Overexpression of PICD was sufficient to induce cell migration, invasion, and EMT. Bioinformatic analysis showed that high expression of PICD target genes including *FOS*, *EFEMP2*, and *MMP13* along with *PRSS14* leads to poor survival outcome, supporting the clinical relevance of our findings.

RIP of Prss14 leads N-terminal PICD to translocate into the nucleus upon shedding

Prss14 undergoes RIP upon shedding to generate PICD which is liberated from the membrane and translocated to the nucleus (Fig. 4-6). The nuclear localization was observed with immunocytochemistry using antibody detecting Prss14 N-terminus but the mechanism of its nuclear translocation did not revealed in this study. In amyloid precursor protein (APP) that is one of the best studied substrate of RIP, intracellular domain is phosphorylated and

this phosphorylation is essential for binding to adaptor protein FE65 and nuclear translocation. Interaction between FE65 and intracellular domain modulates transcription of target genes with nuclear protein Tip60 (Chang et al., 2006; Kimberly et al., 2001; von Rotz et al., 2004). Another well-known substrate is Notch. Its intracellular domain translocates to the nucleus through the Importinβ and binds to DNA-binding protein CSL following activation of transcription (Lubman et al., 2004; Nakahara et al., 2009). Like the APP and Notch, how translocation of EICD is regulated as well as which molecules participate in the transcriptional regulation needs to be further studied.

The apparent size of PICD detected by immunoprecipitation is larger than the expected size. This size difference may result from anomalous migration of short fragment or from posttranslational modification. It is known that the detergents like SDS can bind more preferentially to hydrophobic residues and/or α-helical structure of proteins, causing migration inconsistently to expected position in the gel (Rath et al., 2009). Prss14 cytoplasmic domain possesses two α-helices (Fig. 15A), which is predicted by I-TASSER server (Yang et al., 2015) and is likely to be bound with more detergent, causing increased apparent size. On the other hand, one possible posttranslational modification is SUMOylation. The SUMO modifies many nuclear proteins functioned in transcription, chromatin structure, and DNA repair and regulates their nuclear localization and activity (Johnson, 2004). In PICD sequence, there are two putative

SUMOylation sites (Zhao et al., 2014) that can be SUMOylated *in vitro*.

RIP of Prss14 is mediated by SPPL2b (Fig. 11 and Fig. 12). Inhibition of SPPL2b activity or knockdown of SPPL2b reduced PICD generation (Fig. 9B and Fig. 12), while forced expression of SPPL2b increased it (Fig. 13). Flag-N213 and Flag-FL were more effective substrates for SPPL2b than Flag-N149 and Flag-N162 lacking sheddase cleavage sites (Fig. 14B). Thus, it seems that removing the bulk region of extracellular part is not enough for the SPPL2b-dependent cleavage. Rather, cleavage at the right position may provide a favorable conformational change for access of and cleavage by the RIP protease. In addition, helix-destabilizing residue, Gly73, was found at the conserved position in transmembrane domains of Prss14 and known SPPL2b substrates (Fig. 9A). The transmembrane α-helices of integral membrane proteins usually prevent the access of intramembrane proteases. Presence of Gly73 in the transmembrane helix of Prss14 may reduce the α-helical content of its transmembrane domain, thus exposing the cleavage site for the intramembrane protease (Fluhrer et al., 2012; Lemberg and Martoglio, 2002). PICD was not completely inhibited in the cells expressing G73A. This also observed in similar studies with Bri2 and CD74 (Fluhrer et al., 2012; Huttl et al., 2016). The Bir2 mutant replacing all glycines within the transmembrane region to alanines showed reduced ICD. Though Bri3 that is close homologue of Bri2 contains glycine residues in transmembrane, it is not a substrate for

SPPL2b (Martin et al., 2009). These results demonstrate that the SPPL-mediated cleavage of intramembrane domain is not solely determined by the destabilized secondary structure.

PICD can play key multiple roles during metastasis through transcriptome changes

To screen the PICD-regulated genes, RNA-seq analysis was done with three different sets of conditions (Fig. 16A). The experiments were designed to analyze genes (1) induced by PICD after PMA-mediated shedding, (2) not affected by only PMA without RIP and, (3) induced directly by PICD in SP2bKD cells. Three sets of DEG analyses after removal of genes with not consistent expression directionality yield final 28 genes as PICD target gene candidate (Table 1).

The most of target genes were involved in cellular processes associated with cancer progression and metastasis, such as immune response, cell proliferation, invasion, and angiogenesis (Table 1 and 3). For the verification of PICD functions, cell migration and invasion which were well-known function of Prss14 were tested. Using *in vitro* cell-based assays, it was shown that PICD alone was sufficient to enhance cell migration and invasion (Fig. 21-24).

It is suspected that the PICD-regulated genes may include EMT function since Prss14 is necessary and sufficient for EMT (Lee et al.,

2010). Quick search of online EMT database such as dbEMT (Zhao et al., 2015) did not include the most of genes in the final list 28 genes except *MMP13* and *TNF*. However, literature searches for the individual genes revealed the experimental evidences of 12 genes that are causing EMT. Furthermore, expression of PICD alone induces EMT-like morphological changes (Fig. 25). Flag-N55-overexpressing cells reveal less expression of pre-EMT markers, E-cadherin, and more expression of post-EMT marker, vimentin (Fig. 26).

It is interesting that *FOS* gene appears as a PICD target gene and most of the genes in the final list contain the *FOS* binding sites. In functional network analysis carried out by STRING, *FOS* behaves as a core gene to connect most other transcription factors and also other core genes, *TNF* and *UBC* (Fig. 18 and Fig. 19). FOS is known for directly regulating EMT. FOS can drive mesenchymal morphology as well as transcriptional changes of EMT marker genes, such as *CDH, VIM*, and *SLUG* (Eger et al., 2000; Gao et al., 2015; Mejlvang et al., 2007; Shao et al., 2014). Other transcription factors, ATF3, EGR3, and NR4A1 are also known to be involved in EMT (Chaudhury et al., 2016; Yin et al., 2010; Zhou et al., 2014). Therefore, it is highly likely that *FOS* is the key transcription factor in PICD target genes driving the EMT pathway.

It was also revealed that genes encoding cytokines in the TNF-related pathway are the PICD targets (Table 1). These cytokines were implicated in various aspects of cancer development and

metastasis. They modulate cancer microenvironment for cancer cells to escape the immune response (Kitamura et al., 2015; Schreiber et al., 2011). Especially, the cytokines in PICD target genes are functionally associated with *TNF* in gene networks from STRING (Fig. 18 and Fig. 19). It is well recognized that TNF, a multifunctional cytokine, is produced from cancer cells and plays important roles by regulating cell survival, EMT, and angiogenesis through various signaling pathway in cancer progression and metastasis (Balkwill, 2009; Wu and Zhou, 2010). Also, TNF functions as a key proinflammatory cytokines to promote inflammation that is closely linked cancer development (Balkwill, 2009; Balkwill, 2012). Interestingly, CXCL2 and CXCL3, chemokines well-known for recruiting tumor-associated leukocytes (Galdiero et al., 2013) are induced by TNF (Acharyya et al., 2012; Qiao et al., 2016) and play important roles in metastasis by exerting proangiogenic effect (Acharyya et al., 2012; Sarvaiya et al., 2013; See et al., 2014).

Taken together, it is evident that PICD promotes cancer metastasis by regulating gene expression that involved in various processes including invasion, EMT, and immune modulation, although further studies are required to examine that these PICD target genes indeed function in cancer development and metastasis by PICD.

RIP of Prss14 is better prognosis marker for ER negative

breast cancer

Previously, Prss14 was reported as a significant prognosis marker for ER negative breast cancer that has high medical unmet need (Kim et al., 2016). Triple negative breast cancer is the most aggressive and metastatic subtype and there is no effective targeted therapy available at the clinical level (Wahba and El-Hadaad, 2015). In this study, I expect to extend the significance of Prss14 as a valuable marker for prognosis and therapy of ER-negative breast cancer by identifying RIP process. PICD target genes showed significant enrichment plot in breast cancer patients with high expression of *PRSS14* (Fig. 27). Several genes' expression positively correlated with *SPPL2B* in $PRSS14^{high}$ group (Fig. 28). TACE, another factor required for PICD generation, is upregulated in triple negative breast cancer (McGowan et al., 2013). Therefore, it is speculated that $SPPL2B^{high}$ and $PRSS14^{high}$ group of ER negative breast cancer patients can generate more PICD than $SPPL2B^{low}$ and $PRSS14^{low}$ group.

The critical enzyme for PICD generation, *SPPL2B* contributes survival of *PRSS14* expressing ER negative breast cancer patients. $PRSS14^{high}$ and $SPPL2B^{high}$ group showed the poorest survival in ER negative patients (Fig. 29). In addition, when PICD target genes, *FOS*, *EFEMP2*, and *MMP13,* were highly expressed along with *PRSS14*, the survival rate was significantly poor (Fig. 30). $PRSS14^{high}$ and FOS^{high} group in ER negative patients showed the lowest survival among all the groups. Therefore, it is proposed that at least *FOS*,

EFEMP2, and *MMP13* along with *PRSS14* and *SPPL2B* can be valuable prognosis markers and therapeutic targets of ER negative breast cancer, especially triple negative breast cancer.

Prss14 contributes in metastasis by providing signals from both inside and outside of the cell

It is well documented that Prss14 promotes cancer progression and metastasis through its protease activity against diverse substrates involved in cancer (List, 2009; Uhland, 2006). Prss14 enhances cancer cell invasion, angiogenesis, and metastasis by remodeling extracellular matrix (ECM) through cleavage of ECM molecules as well as activation of uPA and MMP3 (Jin et al., 2006; Lee et al., 2000; Tripathi et al., 2011). Prss14 also activates growth factor and receptors and induces signaling pathways associated with cancer formation and progression, such as PAR2-NFκB, HGF-c-Met, and Tie2 downstream signaling pathway (Kim et al., 2011; List et al., 2005; Sales et al., 2015; Szabo et al., 2011; Zoratti et al., 2016). So far many studies has focused on protease activity of Prss14.

This study presents a novel mechanism that PICD of Prss14 produced by RIP process serves to induce tumor progression and metastasis through transcriptional modulation. The mature Prss14 is shed by TACE upon various stimuli. Active Prss14 promotes ECM degradation and activates its substrates that are associated with cancer progression. Meanwhile, membrane-anchored N-terminal

fragment is further processed by SPPL2b resulting in PICD generation. The PICD translocates to the nucleus and regulates transcription of target genes including transcription factors, cytokines, and genes involved in ubiquitin proteasome pathway. These target genes promote metastasis through induction of EMT and modulation of tumor microenvironment for favorable metastasis. Therefore, Prss14 can function dually in cancer progression and metastasis through both extracellular protease activity and transcriptional regulator (Fig. 31).

REFERENCES

Acharyya, S., Oskarsson, T., Vanharanta, S., Malladi, S., Kim, J., Morris, P. G., Manova-Todorova, K., Leversha, M., Hogg, N., Seshan, V. E.*, et al.* (2012). A CXCL1 paracrine network links cancer chemoresistance and metastasis. Cell *150*, 165-178.

Affara, N. I., Andreu, P., and Coussens, L. M. (2009). Delineating protease functions during cancer development. Methods Mol Biol *539*, 1-32.

Balkwill, F. (2009). Tumour necrosis factor and cancer. Nat Rev Cancer *9*, 361-371.

Balkwill, F. R. (2012). The chemokine system and cancer. J Pathol *226*, 148-157.

Benaud, C., Dickson, R. B., and Lin, C. Y. (2001). Regulation of the activity of matriptase on epithelial cell surfaces by a blood-derived factor. Eur J Biochem *268*, 1439-1447.

Brown, M. S., Ye, J., Rawson, R. B., and Goldstein, J. L. (2000). Regulated intramembrane proteolysis: a control mechanism conserved from bacteria to humans. Cell *100*, 391-398.

Center, B. I. T. G. D. A. (2016). Analysis-ready standardized TCGA data from Broad GDAC Firehose 2016_01_28 run. In Broad Institute of MIT and Harvard. .

Chambers, A. F., Groom, A. C., and MacDonald, I. C. (2002). Dissemination and growth of cancer cells in metastatic sites. Nat Rev Cancer *2*, 563-572.

Chang, K. A., Kim, H. S., Ha, T. Y., Ha, J. W., Shin, K. Y., Jeong, Y. H., Lee, J. P., Park, C. H., Kim, S., Baik, T. K., and Suh, Y. H. (2006). Phosphorylation of amyloid precursor protein (APP) at Thr668 regulates the nuclear translocation of the APP intracellular domain and induces neurodegeneration. Mol Cell Biol *26*, 4327-4338.

Chang, L. H., Pan, S. L., Lai, C. Y., Tsai, A. C., and Teng, C. M. (2013). Activated PAR-2 regulates pancreatic cancer progression through ILK/HIF-alpha-induced TGF-alpha expression and MEK/VEGF-A-mediated angiogenesis. Am J Pathol *183*, 566-575.

Chaudhury, A., Cheema, S., Fachini, J. M., Kongchan, N., Lu, G., Simon, L. M., Wang, T., Mao, S., Rosen, D. G., Ittmann, M. M., *et al.* (2016). CELF1 is a central node in post-transcriptional regulatory programmes underlying EMT. Nat Commun *7*, 13362.

Chen, M., Chen, L. M., Lin, C. Y., and Chai, K. X. (2008). The epidermal growth factor receptor (EGFR) is proteolytically modified by the Matriptase-Prostasin serine protease cascade in cultured epithelial cells. Biochim Biophys Acta *1783*, 896-903.

Cheng, T. S., Chen, W. C., Lin, Y. Y., Tsai, C. H., Liao, C. I., Shyu, H. Y., Ko, C. J., Tzeng, S. F., Huang, C. Y., Yang, P. C., *et al.* (2013). Curcumin-targeting pericellular serine protease matriptase role in suppression of prostate cancer cell invasion, tumor growth, and metastasis. Cancer Prev Res (Phila) *6*, 495-

505.

Cho, E. G., Kim, M. G., Kim, C., Kim, S. R., Seong, I. S., Chung, C., Schwartz, R. H., and Park, D. (2001). N-terminal processing is essential for release of epithin, a mouse type II membrane serine protease. J Biol Chem *276*, 44581-44589.

Cho, E. G., Schwartz, R. H., and Kim, M. G. (2005). Shedding of membrane epithin is blocked without LDLRA4 and its protease activation site. Biochem Biophys Res Commun *327*, 328-334.

Cho, Y., Park, D., and Kim, C. (2017). Disruption of TACE-filamin interaction can inhibit TACE-mediated ectodomain shedding. Biochem Biophys Res Commun *490*, 997-1003.

Chua, H. L., Bhat-Nakshatri, P., Clare, S. E., Morimiya, A., Badve, S., and Nakshatri, H. (2007). NF-kappaB represses E-cadherin expression and enhances epithelial to mesenchymal transition of mammary epithelial cells: potential involvement of ZEB-1 and ZEB-2. Oncogene *26*, 711-724.

Consortium, E. P. (2012). An integrated encyclopedia of DNA elements in the human genome. Nature *489*, 57-74.

Deryugina, E. I., and Quigley, J. P. (2006). Matrix metalloproteinases and tumor metastasis. Cancer Metastasis Rev *25*, 9-34.

Dong, T., Zhang, Y., Chen, Y., Liu, P., An, T., Zhang, J., Yang, H., Zhu, W., and Yang, X. (2017). FOXO1 inhibits the invasion and metastasis of hepatocellular carcinoma by reversing ZEB2-induced epithelial-mesenchymal transition. Oncotarget *8*, 1703-1713.

Eger, A., Stockinger, A., Schaffhauser, B., Beug, H., and Foisner, R. (2000). Epithelial mesenchymal transition by c-Fos estrogen receptor activation involves nuclear translocation of beta-catenin and upregulation of beta-catenin/lymphoid enhancer binding factor-1 transcriptional activity. J Cell Biol *148*, 173-188.

Fluhrer, R., Martin, L., Klier, B., Haug-Kroper, M., Grammer, G., Nuscher, B., and Haass, C. (2012). The alpha-helical content of the transmembrane domain of the British dementia protein-2 (Bri2) determines its processing by signal peptide peptidase-like 2b (SPPL2b). J Biol Chem *287*, 5156-5163.

Fluhrer, R., Steiner, H., and Haass, C. (2009). Intramembrane proteolysis by signal peptide peptidases: a comparative discussion of GXGD-type aspartyl proteases. J Biol Chem *284*, 13975-13979.

Friedl, P., and Wolf, K. (2003). Tumour-cell invasion and migration: diversity and escape mechanisms. Nat Rev Cancer *3*, 362-374.

Friedmann, E., Hauben, E., Maylandt, K., Schleeger, S., Vreugde, S., Lichtenthaler, S. F., Kuhn, P. H., Stauffer, D., Rovelli, G., and Martoglio, B. (2006). SPPL2a and SPPL2b promote intramembrane proteolysis of TNFalpha in activated dendritic cells to trigger IL-12 production. Nat Cell Biol *8*, 843-848.

Friis, S., Sales, K. U., Schafer, J. M., Vogel, L. K., Kataoka, H., and Bugge, T. H. (2014). The protease inhibitor HAI-2, but not HAI-1, regulates matriptase activation and shedding through

prostasin. J Biol Chem *289*, 22319-22332.

Galdiero, M. R., Garlanda, C., Jaillon, S., Marone, G., and Mantovani, A. (2013). Tumor associated macrophages and neutrophils in tumor progression. J Cell Physiol *228*, 1404-1412.

Gao, J., Yan, Q., Wang, J., Liu, S., and Yang, X. (2015). Epithelial-to-mesenchymal transition induced by TGF-beta1 is mediated by AP1-dependent EpCAM expression in MCF-7 cells. J Cell Physiol *230*, 775-782.

Gupta, G. P., and Massague, J. (2006). Cancer metastasis: building a framework. Cell *127*, 679-695.

Ha, S. Y., Kim, K. Y., Lee, N. K., Kim, M. G., and Kim, S. H. (2014). Overexpression of matriptase correlates with poor prognosis in esophageal squamous cell carcinoma. Virchows Arch *464*, 19-27.

Hardy, J., and Selkoe, D. J. (2002). The amyloid hypothesis of Alzheimer's disease: progress and problems on the road to therapeutics. Science *297*, 353-356.

Hedrick, E., and Safe, S. (2017). Transforming Growth Factor beta/NR4A1-Inducible Breast Cancer Cell Migration and Epithelial-to-Mesenchymal Transition Is p38alpha (Mitogen-Activated Protein Kinase 14) Dependent. Mol Cell Biol *37*.

Hsu, Y. T., Osmulski, P., Wang, Y., Huang, Y. W., Liu, L., Ruan, J., Jin, V. X., Kirma, N. B., Gaczynska, M. E., and Huang, T. H. (2016). EpCAM-Regulated Transcription Exerts Influences on Nanomechanical Properties of Endometrial Cancer Cells That

Promote Epithelial-to-Mesenchymal Transition. Cancer Res *76*, 6171-6182.

Huang, S. H., Law, C. H., Kuo, P. H., Hu, R. Y., Yang, C. C., Chung, T. W., Li, J. M., Lin, L. H., Liu, Y. C., Liao, E. C.*, et al.* (2016). MMP-13 is involved in oral cancer cell metastasis (Retracted article.See vol.7,pg.48851,2016). Oncotarget *7*, 17144-17161.

Huttl, S., Helfrich, F., Mentrup, T., Held, S., Fukumori, A., Steiner, H., Saftig, P., Fluhrer, R., and Schroder, B. (2016). Substrate determinants of signal peptide peptidase-like 2a (SPPL2a)-mediated intramembrane proteolysis of the invariant chain CD74. Biochem J *473*, 1405-1422.

Hwang, W., Chiu, Y. F., Kuo, M. H., Lee, K. L., Lee, A. C., Yu, C. C., Chang, J. L., Huang, W. C., Hsiao, S. H., Lin, S. E., and Chou, Y. T. (2017). Expression of Neuroendocrine Factor VGF in Lung Cancer Cells Confers Resistance to EGFR Kinase Inhibitors and Triggers Epithelial-to-Mesenchymal Transition. Cancer Res *77*, 3013-3026.

Ihara, S., Miyoshi, E., Ko, J. H., Murata, K., Nakahara, S., Honke, K., Dickson, R. B., Lin, C. Y., and Taniguchi, N. (2002). Prometastatic effect of N-acetylglucosaminyltransferase V is due to modification and stabilization of active matriptase by adding beta 1-6 GlcNAc branching. J Biol Chem *277*, 16960-16967.

Inouye, K., Tomoishi, M., Yasumoto, M., Miyake, Y., Kojima, K., Tsuzuki, S., and Fushiki, T. (2013). Roles of CUB and LDL

receptor class A domain repeats of a transmembrane serine protease matriptase in its zymogen activation. J Biochem *153*, 51-61.

Inouye, K., Tsuzuki, S., Yasumoto, M., Kojima, K., Mochida, S., and Fushiki, T. (2010). Identification of the matriptase second CUB domain as the secondary site for interaction with hepatocyte growth factor activator inhibitor type-1. J Biol Chem *285*, 33394-33403.

Jin, X., Yagi, M., Akiyama, N., Hirosaki, T., Higashi, S., Lin, C. Y., Dickson, R. B., Kitamura, H., and Miyazaki, K. (2006). Matriptase activates stromelysin (MMP-3) and promotes tumor growth and angiogenesis. Cancer Sci *97*, 1327-1334.

Johnson, E. S. (2004). Protein modification by SUMO. Annu Rev Biochem *73*, 355-382.

Kan, J., Thomson, S., Argast, G. M., O' Connor, M. E., Robinson, M., Feng, B., Heyer, Chiu, M. I., and Nicoletti, R. (2012). Use of EMT gene signitures in cancer drug discovery, diagnostics, and treatment. In, (US: AVEO PHARMACEUTICALS, INC., Cambridge, MA (US); OSI Pharmaceuticals, LLC, Farmingdale, NY (US)).

Kang, J. Y., Dolled-Filhart, M., Ocal, I. T., Singh, B., Lin, C. Y., Dickson, R. B., Rimm, D. L., and Camp, R. L. (2003). Tissue microarray analysis of hepatocyte growth factor/Met pathway components reveals a role for Met, matriptase, and hepatocyte growth factor activator inhibitor 1 in the progression of node-negative breast cancer. Cancer Res *63*, 1101-1105.

Kim, C., Cho, Y., Kang, C. H., Kim, M. G., Lee, H., Cho, E. G., and Park, D. (2005). Filamin is essential for shedding of the transmembrane serine protease, epithin. EMBO Rep *6*, 1045-1051.

Kim, C., Lee, H. S., Lee, D., Lee, S. D., Cho, E. G., Yang, S. J., Kim, S. B., Park, D., and Kim, M. G. (2011). Epithin/PRSS14 proteolytically regulates angiopoietin receptor Tie2 during transendothelial migration. Blood *117*, 1415-1424.

Kim, S., Yang, J. W., Kim, C., and Kim, M. G. (2016). Impact of suppression of tumorigenicity 14 (ST14)/serine protease 14 (Prss14) expression analysis on the prognosis and management of estrogen receptor negative breast cancer. Oncotarget *7*, 34643-34663.

Kim, S. B., Lee, D., Jeong, J. W., Kim, C., Park, D., and Kim, M. G. (2010). Soluble epithin/PRSS14 secreted from cancer cells contains active angiogenic potential. Mol Cells *29*, 617-623.

Kimberly, W. T., Zheng, J. B., Guenette, S. Y., and Selkoe, D. J. (2001). The intracellular domain of the beta-amyloid precursor protein is stabilized by Fe65 and translocates to the nucleus in a notch-like manner. J Biol Chem *276*, 40288-40292.

Kitamura, T., Qian, B. Z., and Pollard, J. W. (2015). Immune cell promotion of metastasis. Nat Rev Immunol *15*, 73-86.

Ko, C. J., Huang, C. C., Lin, H. Y., Juan, C. P., Lan, S. W., Shyu, H. Y., Wu, S. R., Hsiao, P. W., Huang, H. P., Shun, C. T., and Lee, M. S. (2015). Androgen-Induced TMPRSS2 Activates

Matriptase and Promotes Extracellular Matrix Degradation, Prostate Cancer Cell Invasion, Tumor Growth, and Metastasis. Cancer Res *75*, 2949-2960.

Krawitz, P., Haffner, C., Fluhrer, R., Steiner, H., Schmid, B., and Haass, C. (2005). Differential localization and identification of a critical aspartate suggest non-redundant proteolytic functions of the presenilin homologues SPPL2b and SPPL3. J Biol Chem *280*, 39515-39523.

Lal, M., and Caplan, M. (2011). Regulated intramembrane proteolysis: signaling pathways and biological functions. Physiology (Bethesda) *26*, 34-44.

Lee, D., Lee, H. S., Yang, S. J., Jeong, H., Kim, D. Y., Lee, S. D., Oh, J. W., Park, D., and Kim, M. G. (2011). PRSS14/Epithin is induced in macrophages by the IFN-gamma/JAK/STAT pathway and mediates transendothelial migration. Biochem Biophys Res Commun *405*, 644-650.

Lee, H. S., Kim, C., Kim, S. B., Kim, M. G., and Park, D. (2010). Epithin, a target of transforming growth factor-beta signaling, mediates epithelial-mesenchymal transition. Biochem Biophys Res Commun *395*, 553-559.

Lee, H. S., Park, B. M., Cho, Y., Kim, S., Kim, C., Kim, M. G., and Park, D. (2014). Shedding of epithin/PRSS14 is induced by TGF-beta and mediated by tumor necrosis factor-alpha converting enzyme. Biochem Biophys Res Commun *452*, 1084-1090.

Lee, J. W., Yong Song, S., Choi, J. J., Lee, S. J., Kim, B. G., Park,

C. S., Lee, J. H., Lin, C. Y., Dickson, R. B., and Bae, D. S. (2005). Increased expression of matriptase is associated with histopathologic grades of cervical neoplasia. Hum Pathol *36*, 626-633.

Lee, S. L., Dickson, R. B., and Lin, C. Y. (2000). Activation of hepatocyte growth factor and urokinase/plasminogen activator by matriptase, an epithelial membrane serine protease. J Biol Chem *275*, 36720-36725.

Lemberg, M. K., and Martoglio, B. (2002). Requirements for signal peptide peptidase-catalyzed intramembrane proteolysis. Mol Cell *10*, 735-744.

Lichtenthaler, S. F., Haass, C., and Steiner, H. (2011). Regulated intramembrane proteolysis--lessons from amyloid precursor protein processing. J Neurochem *117*, 779-796.

Lin, C. W., Liao, M. Y., Lin, W. W., Wang, Y. P., Lu, T. Y., and Wu, H. C. (2012). Epithelial cell adhesion molecule regulates tumor initiation and tumorigenesis via activating reprogramming factors and epithelial-mesenchymal transition gene expression in colon cancer. J Biol Chem *287*, 39449-39459.

Lin, C. Y., Anders, J., Johnson, M., and Dickson, R. B. (1999). Purification and characterization of a complex containing matriptase and a Kunitz-type serine protease inhibitor from human milk. J Biol Chem *274*, 18237-18242.

Lin, C. Y., Tseng, I. C., Chou, F. P., Su, S. F., Chen, Y. W., Johnson, M. D., and Dickson, R. B. (2008). Zymogen activation,

inhibition, and ectodomain shedding of matriptase. Front Biosci *13*, 621-635.

List, K. (2009). Matriptase: a culprit in cancer? Future Oncol *5*, 97-104.

List, K., Bugge, T. H., and Szabo, R. (2006). Matriptase: potent proteolysis on the cell surface. Mol Med *12*, 1-7.

List, K., Szabo, R., Molinolo, A., Sriuranpong, V., Redeye, V., Murdock, T., Burke, B., Nielsen, B. S., Gutkind, J. S., and Bugge, T. H. (2005). Deregulated matriptase causes ras-independent multistage carcinogenesis and promotes ras-mediated malignant transformation. Genes Dev *19*, 1934-1950.

Lourenco, A. R., and Coffer, P. J. (2017). SOX4: Joining the Master Regulators of Epithelial-to-Mesenchymal Transition? Trends Cancer *3*, 571-582.

Lubman, O. Y., Korolev, S. V., and Kopan, R. (2004). Anchoring notch genetics and biochemistry; structural analysis of the ankyrin domain sheds light on existing data. Mol Cell *13*, 619-626.

Maetzel, D., Denzel, S., Mack, B., Canis, M., Went, P., Benk, M., Kieu, C., Papior, P., Baeuerle, P. A., Munz, M., and Gires, O. (2009). Nuclear signalling by tumour-associated antigen EpCAM. Nat Cell Biol *11*, 162-171.

Martin, L., Fluhrer, R., and Haass, C. (2009). Substrate requirements for SPPL2b-dependent regulated intramembrane proteolysis. J Biol Chem *284*, 5662-5670.

McGowan, P. M., Mullooly, M., Caiazza, F., Sukor, S., Madden,

S. F., Maguire, A. A., Pierce, A., McDermott, E. W., Crown, J., O'Donovan, N., and Duffy, M. J. (2013). ADAM-17: a novel therapeutic target for triple negative breast cancer. Ann Oncol *24*, 362-369.

Mejlvang, J., Kriajevska, M., Berditchevski, F., Bronstein, I., Lukanidin, E. M., Pringle, J. H., Mellon, J. K., and Tulchinsky, E. M. (2007). Characterization of E-cadherin-dependent and -independent events in a new model of c-Fos-mediated epithelial-mesenchymal transition. Exp Cell Res *313*, 380-393.

Mohamed, M. M., and Sloane, B. F. (2006). Cysteine cathepsins: multifunctional enzymes in cancer. Nat Rev Cancer *6*, 764-775.

Nakahara, J., Kanekura, K., Nawa, M., Aiso, S., and Suzuki, N. (2009). Abnormal expression of TIP30 and arrested nucleocytoplasmic transport within oligodendrocyte precursor cells in multiple sclerosis. J Clin Invest *119*, 169-181.

Netzel-Arnett, S., Currie, B. M., Szabo, R., Lin, C. Y., Chen, L. M., Chai, K. X., Antalis, T. M., Bugge, T. H., and List, K. (2006). Evidence for a matriptase-prostasin proteolytic cascade regulating terminal epidermal differentiation. J Biol Chem *281*, 32941-32945.

Netzel-Arnett, S., Hooper, J. D., Szabo, R., Madison, E. L., Quigley, J. P., Bugge, T. H., and Antalis, T. M. (2003). Membrane anchored serine proteases: a rapidly expanding group of cell surface proteolytic enzymes with potential roles in cancer. Cancer Metastasis Rev *22*, 237-258.

Nikitin, A., Egorov, S., Daraselia, N., and Mazo, I. (2003).

Pathway studio--the analysis and navigation of molecular networks. Bioinformatics *19*, 2155-2157.

Oberst, M., Anders, J., Xie, B., Singh, B., Ossandon, M., Johnson, M., Dickson, R. B., and Lin, C.-Y. (2001). Matriptase and HAI-1 Are Expressed by Normal and Malignant Epithelial Cells in Vitro and in Vivo. The American Journal of Pathology *158*, 1301-1311.

Oberst, M. D., Johnson, M. D., Dickson, R. B., Lin, C. Y., Singh, B., Stewart, M., Williams, A., al-Nafussi, A., Smyth, J. F., Gabra, H., and Sellar, G. C. (2002). Expression of the serine protease matriptase and its inhibitor HAI-1 in epithelial ovarian cancer: correlation with clinical outcome and tumor clinicopathological parameters. Clin Cancer Res *8*, 1101-1107.

Okada, T., Sinha, S., Esposito, I., Schiavon, G., Lopez-Lago, M. A., Su, W., Pratilas, C. A., Abele, C., Hernandez, J. M., Ohara, M., *et al.* (2015). The Rho GTPase Rnd1 suppresses mammary tumorigenesis and EMT by restraining Ras-MAPK signalling. Nat Cell Biol *17*, 81-94.

Qiao, Y., He, H., Jonsson, P., Sinha, I., Zhao, C., and Dahlman-Wright, K. (2016). AP-1 Is a Key Regulator of Proinflammatory Cytokine TNFalpha-mediated Triple-negative Breast Cancer Progression. J Biol Chem *291*, 5068-5079.

Rath, A., Glibowicka, M., Nadeau, V. G., Chen, G., and Deber, C. M. (2009). Detergent binding explains anomalous SDS-PAGE migration of membrane proteins. Proc Natl Acad Sci U S A *106*,

1760-1765.

Robinson, M. D., McCarthy, D. J., and Smyth, G. K. (2010). edgeR: a Bioconductor package for differential expression analysis of digital gene expression data. Bioinformatics *26*, 139-140.

Saleem, M., Adhami, V. M., Zhong, W., Longley, B. J., Lin, C. Y., Dickson, R. B., Reagan-Shaw, S., Jarrard, D. F., and Mukhtar, H. (2006). A novel biomarker for staging human prostate adenocarcinoma: overexpression of matriptase with concomitant loss of its inhibitor, hepatocyte growth factor activator inhibitor-1. Cancer Epidemiol Biomarkers Prev *15*, 217-227.

Sales, K. U., Friis, S., Konkel, J. E., Godiksen, S., Hatakeyama, M., Hansen, K. K., Rogatto, S. R., Szabo, R., Vogel, L. K., Chen, W.*, et al.* (2015). Non-hematopoietic PAR-2 is essential for matriptase-driven pre-malignant progression and potentiation of ras-mediated squamous cell carcinogenesis. Oncogene *34*, 346-356.

Sarvaiya, P. J., Guo, D., Ulasov, I., Gabikian, P., and Lesniak, M. S. (2013). Chemokines in tumor progression and metastasis. Oncotarget *4*, 2171-2185.

Schreiber, R. D., Old, L. J., and Smyth, M. J. (2011). Cancer immunoediting: integrating immunity's roles in cancer suppression and promotion. Science *331*, 1565-1570.

See, A. L., Chong, P. K., Lu, S. Y., and Lim, Y. P. (2014). CXCL3 is a potential target for breast cancer metastasis. Curr Cancer

Drug Targets *14*, 294-309.
Sevenich, L., and Joyce, J. A. (2014). Pericellular proteolysis in cancer. Genes Dev *28*, 2331-2347.
Shan, Y., You, B., Shi, S., Shi, W., Zhang, Z., Zhang, Q., Gu, M., Chen, J., Bao, L., Liu, D., and You, Y. (2018). Hypoxia-Induced Matrix Metalloproteinase-13 Expression in Exosomes from Nasopharyngeal Carcinoma Enhances Metastases. Cell Death Dis *9*, 382.
Shao, D. D., Xue, W., Krall, E. B., Bhutkar, A., Piccioni, F., Wang, X., Schinzel, A. C., Sood, S., Rosenbluh, J., Kim, J. W., *et al.* (2014). KRAS and YAP1 converge to regulate EMT and tumor survival. Cell *158*, 171-184.
Steinmetzer, T., Schweinitz, A., Sturzebecher, A., Donnecke, D., Uhland, K., Schuster, O., Steinmetzer, P., Muller, F., Friedrich, R., Than, M. E., *et al.* (2006). Secondary amides of sulfonylated 3-amidinophenylalanine. New potent and selective inhibitors of matriptase. J Med Chem *49*, 4116-4126.
Subramanian, A., Tamayo, P., Mootha, V. K., Mukherjee, S., Ebert, B. L., Gillette, M. A., Paulovich, A., Pomeroy, S. L., Golub, T. R., Lander, E. S., and Mesirov, J. P. (2005). Gene set enrichment analysis: a knowledge-based approach for interpreting genome-wide expression profiles. Proc Natl Acad Sci U S A *102*, 15545-15550.
Szabo, R., Hobson, J. P., List, K., Molinolo, A., Lin, C. Y., and Bugge, T. H. (2008). Potent inhibition and global co-localization implicate the transmembrane Kunitz-type serine

protease inhibitor hepatocyte growth factor activator inhibitor-2 in the regulation of epithelial matriptase activity. J Biol Chem *283*, 29495-29504.

Szabo, R., Rasmussen, A. L., Moyer, A. B., Kosa, P., Schafer, J. M., Molinolo, A. A., Gutkind, J. S., and Bugge, T. H. (2011). c-Met-induced epithelial carcinogenesis is initiated by the serine protease matriptase. Oncogene *30*, 2003-2016.

Szklarczyk, D., Franceschini, A., Wyder, S., Forslund, K., Heller, D., Huerta-Cepas, J., Simonovic, M., Roth, A., Santos, A., Tsafou, K. P.*, et al.* (2015). STRING v10: protein-protein interaction networks, integrated over the tree of life. Nucleic Acids Res *43*, D447-452.

Takeuchi, T., Harris, J. L., Huang, W., Yan, K. W., Coughlin, S. R., and Craik, C. S. (2000). Cellular localization of membrane-type serine protease 1 and identification of protease-activated receptor-2 and single-chain urokinase-type plasminogen activator as substrates. J Biol Chem *275*, 26333-26342.

Thiery, J. P. (2002). Epithelial-mesenchymal transitions in tumour progression. Nat Rev Cancer *2*, 442-454.

Tripathi, M., Potdar, A. A., Yamashita, H., Weidow, B., Cummings, P. T., Kirchhofer, D., and Quaranta, V. (2011). Laminin-332 cleavage by matriptase alters motility parameters of prostate cancer cells. Prostate *71*, 184-196.

Tsai, C. H., Teng, C. H., Tu, Y. T., Cheng, T. S., Wu, S. R., Ko, C. J., Shyu, H. Y., Lan, S. W., Huang, H. P., Tzeng, S. F.*, et al.* (2014). HAI-2 suppresses the invasive growth and metastasis

of prostate cancer through regulation of matriptase. Oncogene *33*, 4643-4652.

Tseng, C. C., Jia, B., Barndt, R., Gu, Y., Chen, C. Y., Tseng, I. C., Su, S. F., Wang, J. K., Johnson, M. D., and Lin, C. Y. (2017). Matriptase shedding is closely coupled with matriptase zymogen activation and requires de novo proteolytic cleavage likely involving its own activity. PLoS One *12*, e0183507.

Uhland, K. (2006). Matriptase and its putative role in cancer. Cell Mol Life Sci *63*, 2968-2978.

von Rotz, R. C., Kohli, B. M., Bosset, J., Meier, M., Suzuki, T., Nitsch, R. M., and Konietzko, U. (2004). The APP intracellular domain forms nuclear multiprotein complexes and regulates the transcription of its own precursor. J Cell Sci *117*, 4435-4448.

Voon, D. C., and Thiery, J. P. (2017). The Emerging Roles of RUNX Transcription Factors in Epithelial-Mesenchymal Transition. Adv Exp Med Biol *962*, 471-489.

Voss, M., Schroder, B., and Fluhrer, R. (2013). Mechanism, specificity, and physiology of signal peptide peptidase (SPP) and SPP-like proteases. Biochim Biophys Acta *1828*, 2828-2839.

Wahba, H. A., and El-Hadaad, H. A. (2015). Current approaches in treatment of triple-negative breast cancer. Cancer Biol Med *12*, 106-116.

Wang, C., Ruan, P., Zhao, Y., Li, X., Wang, J., Wu, X., Liu, T., Wang, S., Hou, J., Li, W., *et al.* (2017). Spermidine/spermine N1-acetyltransferase regulates cell growth and metastasis via

AKT/beta-catenin signaling pathways in hepatocellular and colorectal carcinoma cells. Oncotarget *8*, 1092-1109.

Wang, H., Wang, H. S., Zhou, B. H., Li, C. L., Zhang, F., Wang, X. F., Zhang, G., Bu, X. Z., Cai, S. H., and Du, J. (2013). Epithelial-mesenchymal transition (EMT) induced by TNF-alpha requires AKT/GSK-3beta-mediated stabilization of snail in colorectal cancer. PLoS One *8*, e56664.

Wang, J. K., Lee, M. S., Tseng, I. C., Chou, F. P., Chen, Y. W., Fulton, A., Lee, H. S., Chen, C. J., Johnson, M. D., and Lin, C. Y. (2009). Polarized epithelial cells secrete matriptase as a consequence of zymogen activation and HAI-1-mediated inhibition. Am J Physiol Cell Physiol *297*, C459-470.

Weihofen, A., and Martoglio, B. (2003). Intramembrane-cleaving proteases: controlled liberation of proteins and bioactive peptides. Trends Cell Biol *13*, 71-78.

Welm, A. L., Sneddon, J. B., Taylor, C., Nuyten, D. S., van de Vijver, M. J., Hasegawa, B. H., and Bishop, J. M. (2007). The macrophage-stimulating protein pathway promotes metastasis in a mouse model for breast cancer and predicts poor prognosis in humans. Proc Natl Acad Sci U S A *104*, 7570-7575.

Wu, Y., and Zhou, B. P. (2010). TNF-alpha/NF-kappaB/Snail pathway in cancer cell migration and invasion. Br J Cancer *102*, 639-644.

Yang, J., and Weinberg, R. A. (2008). Epithelial-mesenchymal transition: at the crossroads of development and tumor metastasis. Dev Cell *14*, 818-829.

Yang, J., Yan, R., Roy, A., Xu, D., Poisson, J., and Zhang, Y. (2015). The I-TASSER Suite: protein structure and function prediction. Nat Methods *12*, 7-8.

Yin, X., Wolford, C. C., Chang, Y. S., McConoughey, S. J., Ramsey, S. A., Aderem, A., and Hai, T. (2010). ATF3, an adaptive-response gene, enhances TGF{beta} signaling and cancer-initiating cell features in breast cancer cells. J Cell Sci *123*, 3558-3565.

Zhang, D., Wang, S., Chen, J., Liu, H., Lu, J., Jiang, H., Huang, A., and Chen, Y. (2017). Fibulin-4 promotes osteosarcoma invasion and metastasis by inducing epithelial to mesenchymal transition via the PI3K/Akt/mTOR pathway. Int J Oncol *50*, 1513-1530.

Zhao, M., Kong, L., Liu, Y., and Qu, H. (2015). dbEMT: an epithelial-mesenchymal transition associated gene resource. Sci Rep *5*, 11459.

Zhao, Q., Xie, Y., Zheng, Y., Jiang, S., Liu, W., Mu, W., Liu, Z., Zhao, Y., Xue, Y., and Ren, J. (2014). GPS-SUMO: a tool for the prediction of sumoylation sites and SUMO-interaction motifs. Nucleic Acids Res *42*, W325-330.

Zhou, F., Drabsch, Y., Dekker, T. J., de Vinuesa, A. G., Li, Y., Hawinkels, L. J., Sheppard, K. A., Goumans, M. J., Luwor, R. B., de Vries, C. J.*, et al.* (2014). Nuclear receptor NR4A1 promotes breast cancer invasion and metastasis by activating TGF-beta signalling. Nat Commun *5*, 3388.

Zoratti, G. L., Tanabe, L. M., Hyland, T. E., Duhaime, M. J.,

Colombo, E., Leduc, R., Marsault, E., Johnson, M. D., Lin, C. Y., Boerner, J., *et al.* (2016). Matriptase regulates c-Met mediated proliferation and invasion in inflammatory breast cancer. Oncotarget *7*, 58162-58173.

Zoratti, G. L., Tanabe, L. M., Varela, F. A., Murray, A. S., Bergum, C., Colombo, E., Lang, J. E., Molinolo, A. A., Leduc, R., Marsault, E., *et al.* (2015). Targeting matriptase in breast cancer abrogates tumour progression via impairment of stromal-epithelial growth factor signalling. Nat Commun *6*, 6776.

국문초록

막단백질분해효소인 Prss14은 다양한 상피세포암에 과발현되어 있으며, 그것이 암의 발생과, 진행, 전이에 매우 중요한 역할을 한다는 것이 보고되어있다. Prss14은 serum, TGF-β, PMA 등 다양한 자극에 의해서 ectodomain shedding이 일어나는데, 그 이후 membrane에 남겨진 N-말단단편에 대해서는 알려진 바가 없다. 본 연구에서는 Prss14이 shedding된 이후, regulated intramembrane proteolysis에 의해 잘려서 intracellular domain (PICD)이 만들어진다는 것을 밝혔다. PMA를 처리하면 TACE에 의해 Prss14의 ectodomain shedding이 일어나고 SPPL2b는 membrane에 남아있는 N-terminal fragment를 자른다. 이렇게 만들어진 PICD는 membrane에서 떨어져나와, 핵으로 이동하여 전사조절에 관여한다. RNA-sequencing에 의한 전사체분석을 통하여 PICD의 타겟유전자가 전사인자, 사이토카인, 세포의 이동과 침습에 관여하는 유전자, ubiquitin proteasome pathway에 관련된 유전자들을 포함하고 있다는 것을 밝혔다. 이들 유전자는 Fos, Tnf, Ubc 유전자들을 중심으로 기능적인 network를 이루고 있다. 또한, PICD 타겟 유전자들이 세포의 이동, 침습, epithelial-mesenchymal transition (EMT), 암 미세환경 조절을 포함한 암과 관련된 기작에 관여하고 있다는 것을 확인하였다. PICD를 발현시킨 세포에서는 EMT에서 보이는 세포의 모양이 변화가 관찰되었고, pre-EMT marker인 E-cadherin의 발현이 감소하고 post-EMT marker인 Viment의 발현이 증가하였다. 더나아가, PICD를 발현하는 세포에서는 세포의 이동과 침습성이 증가하는 것을 관찰하였다. 세포의 이동과

침습은 SPPL2b를 knockdown하여 PICD가 적게 만들어지는 세포에서는 감소해 있었으며, control 세포에서 관찰되는 PMA에 의한 세포 이동과 침습이 SPPL2b-KD 세포에서는 관찰되지 않았다. 또한 PMA를 처리하지 않아도 SPPL2b-KD 세포에 PICD만 발현시켜도 세포의 이동과 침습이 증가하는 것을 통해 세포의 이동과 침습이 PICD에 의존적으로 조절됨을 확인하였다. Prss14이 과발현되어 있으며, 과발현정도가 암의 진행과 암환자의 생존율에 관련이 있다고 알려져있는 유방암 환자에서 PICD가 만들어지는 현상의 clinical relevance를 확인하였다. 유방암 환자에서 Prss14이 높을 때 PICD 타겟 유전자들의 발현이 통계적으로 유의하게 높았다. 또한, TCGA 유방암 환자의 데이터를 이용한 생존율 분석을 통해서 SPPL2b와 PICD의 타겟유전자들이 Prss14과 함께 높게 발현될 때 ER-negative 유방암 환자에서 생존율이 크게 감소하는 것을 확인하였다. 따라서 Prss14 뿐만 아니라, SPPL2b와 PICD 타겟유전자들은 ER-negative 유방암 환자의 유용한 진단 마커로 쓰일 수 있으며 치료 타켓이 될 수 있음을 알 수 있다. 본 연구는 막단백질분해효소인 Prss14이 타겟유전자들의 전사에 관여하여 암 전이를 조절하는 새로운 기능을 밝혔고, 이 조절기작이 암 환자에게서도 중요함을 제시하였다.